2018

An experimental study of lead and zinc solubility in a hydrothermal fluid

Marlena Joyce Rock

ABSTRACT

AN EXPERIMENTAL STUDY OF LEAD AND ZINC SOLUBILITY IN A HYDROTHERMAL FLUID

Marlena Joyce Rock, M.S.
Department of Geology and Environmental Geosciences
Northern Illinois University, 2018
Dr. Mark Frank, Director

Lead and zinc mineralization has been documented in low-temperature Mississippi Valley Type (MVT) deposits and high-temperature porphyry systems. These deposits are characterized by the presence of galena (PbS) and sphalerite (ZnS) that formed from a salt-bearing hydrothermal fluid. The lead and zinc are most likely transported as $PbCl_2$ and $ZnCl_2$ before precipitating as galena and sphalerite through a decrease in temperature, an increase in pH, or the addition of reduced sulfur. The HCl concentration (pH) of the hydrothermal fluid plays a major role in the concentration of lead and zinc carried in the fluid; however, there are few data detailing the solubility of galena and zinc in acidic hydrothermal fluids at temperatures applicable to MVT and porphyry systems.

Experiments were conducted in René 41 cold-seal pressure vessels from 200 to 500°C and 100 MPa to determine the concentrations of lead and zinc in hydrothermal fluids as a function of HCl. Platinum capsules were loaded with natural galena and sphalerite and an aqueous fluid of 13 to 15 wt.% $NaCl_{eq.}$ containing HCl + NaCl + H_2O. The aqueous fluids were captured at the conclusion of the experiment and lead and zinc concentrations were determined by using AA and ICP-OES.

Lead concentrations were $1.1(\pm0.1)x10^{1}$ μg/g (HCl = $4.68x10^{3}$ μg/g), $1.6(\pm0.2)x10^{1}$ (HCl = $5.35x10^{4}$ μg/g), and $7.9(\pm0.5)x10^{3}$ μg/g (HCl = $5.35x10^{4}$ μg/g) at 200, 300, and 500 °C, respectively. Zinc concentrations were found to be $1.3(\pm0.1)x10^{3}$ μg/g (HCl = $9.36x10^{3}$ μg/g), $2.4(\pm0.3)x10^{3}$ μg/g (HCl = $5.35x10^{4}$ μg/g), and $2.6(\pm0.3)x10^{3}$ μg/g (HCl = $5.35x10^{4}$ μg/g), respectively. The data demonstrate that the concentration of lead and zinc in the fluid increased directly with temperature and HCl concentration. Therefore, decreasing temperature and HCl (increase pH) are efficient at inducing the precipitation of galena and/or sphalerite in MVT and porphyry systems. The variable Pb:Zn ratios observed in some ore-bearing systems are possibly the result of differences in the rate of change of temperature, acidity, and/or reduced sulfur.

NORTHERN ILLINOIS UNIVERSITY
DEKALB, ILLINOIS

MAY 2018

AN EXPERIMENTAL STUDY OF LEAD AND ZINC SOLUBILITY IN A HYDROTHERMAL FLUID

BY

MARLENA JOYCE ROCK

A THESIS SUBMITTED TO THE GRADUATE SCHOOL

IN PARTIAL FULFILLMENT OF THE REQUIREMENTS

FOR THE DEGREE

MASTER OF SCIENCE

DEPARTMENT OF GEOLOGY AND ENVIRONMENTAL GEOSCIENCES

Thesis Director:
Associate Professor Mark R. Frank

ACKNOWLEDGEMENTS

The author would like to acknowledge and thank the partial funding provided from the Ira Edgar Odom scholarship, Northern Illinois University Goldich Fund, and Geological Society of America Research Grant. Joshua Ehlich for his knowledge and assistance in the hydrothermal laboratory, Josh Schwartz for his help with the scanning electron microscope, and Mark Howland for his assistance drafting figures. I would like to acknowledge my committee, Professor Mark Frank, Professor Jim Walker, and Professor Phil Carpenter, for their direction and insight towards my thesis. My undergraduate advisor and friend, Dr. Kurt Friehauf, who introduced me to the wonders of geochemistry and economic geology deserves special thanks. Finally, I would like to thank my advisor, Dr. Mark Frank, for his immense knowledge, guidance, patience, and humor.

DEDICATION

To my parents, Al and LeAnn Rock, who taught me to be my best.

TABLE OF CONTENTS

LIST OF TABLES

Table Page

LIST OF FIGURES

Figure Page

CHAPTER I

INTRODUCTION

Lead (Pb) and zinc (Zn) are important industrial metals. Lead is used predominantly in lead-acid storage batteries and zinc is a main component of brass and bronze. Although these metals are hugely important, they are sparsely distributed in the Earth's crust with average concentrations only ranging from 55 to 75 μg/g (Robb, 2005). Nevertheless, portions of the Earth's crust are mined commercially where elevated concentrations of these economically valuable metals are found. Lead and zinc are typically exploitable at a 5% grade which requires an enrichment factor of 700 times the average concentrations (Robb, 2005). In 2017, $4.7x10^9$ and $13.2x10^9$ tons of lead and zinc were mined, respectively. Hydrothermal lead and zinc deposits are the most common type of ore deposits and are so named because the metals precipitate directly from a hydrothermal fluid due to a change in temperature, pressure, or the composition of the fluid. Lead and zinc are found in a variety of hydrothermal deposits, including porphyry and Mississippi Valley-type (MVT) deposits (Figure 1) and occur most commonly as galena (PbS) and sphalerite (ZnS), respectively.

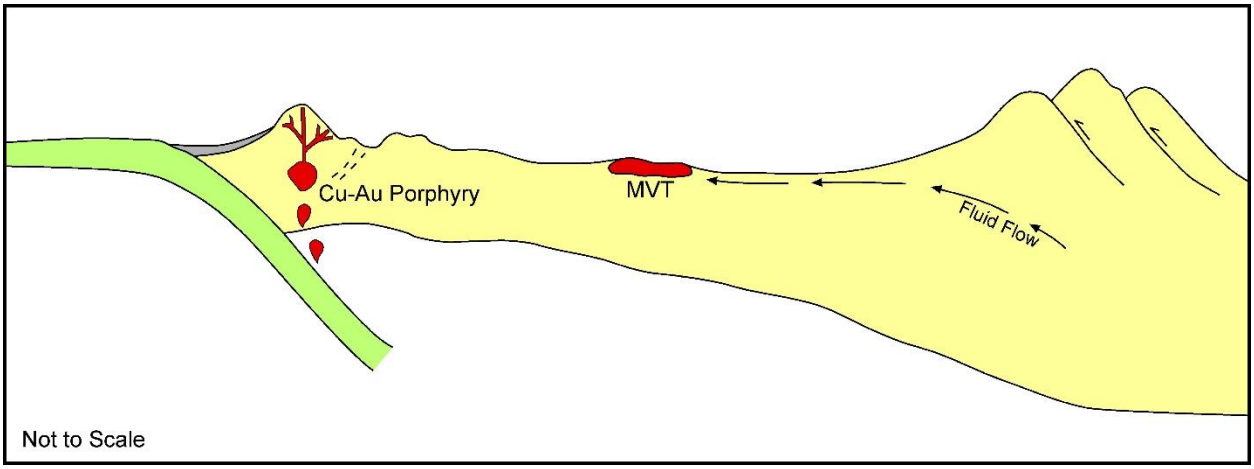

Figure 1: A schematic illustration of geological environments associated with porphyry and MVT deposits. Porphyries are associated with subduction zones and arc-type magmatism. MVT deposits have a hydrological connection between a compressional mountain belt

Mississippi Valley-type Deposits

MVT deposits contain substantial proportions of galena and sphalerite. MVT deposits are found throughout the world with the type locality in the Paleozoic sedimentary rocks of the greater Mississippi Valley region. MVT ores are epigenetic and metal can be deposited tens of millions of years after sediment deposition (e.g. Sverjensky, 1981; Garven & Appold, 1998; Leach et al., 2010). These deposits formed from large volume fluid migrations through foreland basins, driven by compression and topography-driven flow produced by orogenic belts (Figure 1 and 2). The initial compression at the active margin initiates fluid flow and is essential in the early stages for the development of deep, metal-rich, saline, sedimentary brines needed for MVT deposits. After the brines are transported updip, topography-driven flow becomes the principal mechanism for moving fluids over long distances into the foreland basin (Figure 3) (Garven, 1995; Bradley & Leach, 2003; Leach et al., 2010).

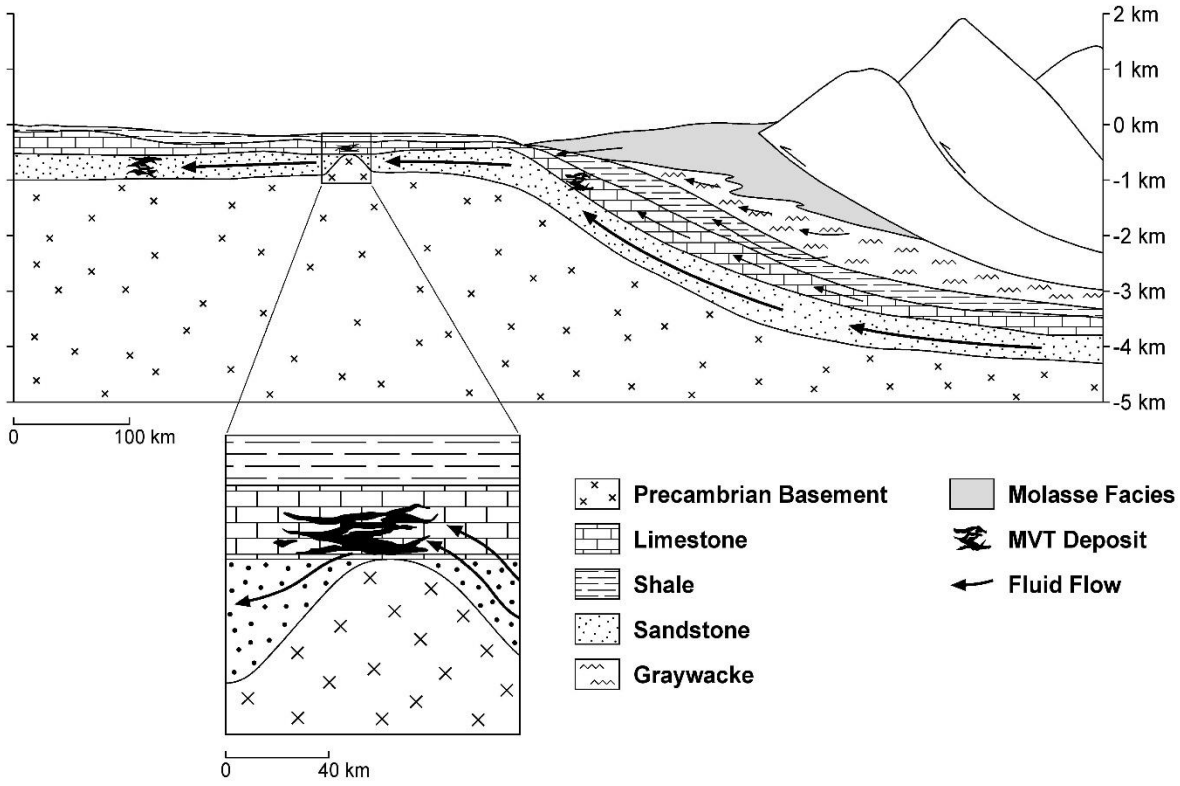

Figure 2: A schematic illustration of the hydrological connection between a compressional mountain belt and a foreland sedimentary basin through which compression and topography drive fluid flow. These areas typify those in which MVT deposits form (modified from Bradley & Leach, 2003).

MVT always occur in areas of mild deformation, expressed in broad domes and basins, gentle folds, and brittle fractures. These deposits primarily occur at shallow depths in limestone or dolostone, and at generally less than 600 meters relative to the surface (Sverjensky, 1986; Leach et al., 2010). The precipitation of metals is hypothesized to be a result of reducing the acidity of the fluid (increasing pH) and/or the addition of reduced sulfur into the system. Hanor (1994, 1996) suggested the fluids depositing main stage mineralization were Na-Ca-Cl, high salinity, low sulfate brines with a pH between 3.5 and 4.5. Fluid inclusion data (e.g. Sverjensky, 1986; Stoffell et al., 2005; Appold & Wenz, 2011; Pelch et al., 2015) suggest the total salinity in these hydrothermal fluids range from 10 to 30 wt.% with homogenization temperatures generally

in the range of 50 to 300°C (Sverjensky, 1986). Highly localized ores and vein mineralization characterize MVT deposits, while local strata control the ore distribution. Elevated concentrations of barium, fluorine, and sulfur are also associated with MVT deposits (Sverjensky, 1981).

Porphyry Deposits

Porphyry systems are magmatic-hydrothermal style deposits associated with porphyritic calk-alkaline or I-type granites. The felsic to intermediate melts are generated adjacent to Andean-type subduction zones (Figure 1). A water-rich hydrothermal fluid is exsolved from the melt through either decompression and/or the crystallization of anhydrous phases (Bodnar et al., 1985). The water-rich hydrothermal fluid contains metals (i.e. Cu, Au, Ag, Mo, Fe, Pb, Zn) derived from the magma and subsequently transports them to shallower depths. The introduction of hydrothermal fluid into the cupola of the porphyry systems results in over-pressurization and the brittle failure of surrounding country rock. The hydrofracturing event allows the metal-rich fluid to move to shallower and cooler stratigraphic locations (i.e. Williams-Jones & Heinrich, 2005; Sillitoe, 2010). The movement of the hydrothermal fluid is vertical from the porphyry stock, with additional lateral flow facilitated via lithologic, structural, and/or hydrothermally induced permeability (Sillitoe, 2010).

From fluid inclusion data of sphalerite veins in porphyry deposits, the fluid carrying the base metal was at a minimum of between 200 and 600°C with a salinity between 2 to 12 wt.% NaCl at the time of deposition (e.g. Lawley et al., 2010; Sillitoe, 2010; Catchpole et al., 2011). Lead and zinc precipitate as a result of fluid neutralization and/or cooling of the hydrothermal fluid as it moves away from the intrusion is especially important (Meinert et al., 2003; Sillitoe,

2010). The cores of porphyry deposits are typically copper-, molybdenum-, and/or gold-rich and contain bornite ± chalcopyrite ± pyrite with lead and zinc mineralization, occurring as galena and sphalerite, along edges of the deposits (Figure 3). Lead and zinc in porphyry deposits are less valuable than the copper, gold, silver, iron or molybdenum and are most often located outside the main body of mineralization in distal skarns, carbonate-replacement and/or sub-epithermal vein deposits (Sillitoe, 2010; Catchpole et al., 2011). Galena and sphalerite are usually found associated with propylitic alteration as a result of the magmatic volatile phase interacting with the country rock and causing metamorphic metasomatism (Figure 3). When the metals are found within the main ore body near the causative igneous intrusion, carbonate host rock are present and the ore deposits are classified as a skarn. These carbonate rock-hosted ores are usually present beneath relatively impermeable rock units and are commonly strata bound with fault control being a significant factor. There appears to be strong connection between the presence of a carbonate host rock and the occurrence of base metal mineralization (Sillitoe, 2010). Most research suggests that the occurrence of lead and zinc in the porphyry zone is a direct result of acid neutralization by the highly reactive carbonate host rocks (Meinert, 1987, 1992; Titley, 1996; Sillitoe, 1997, 2000).

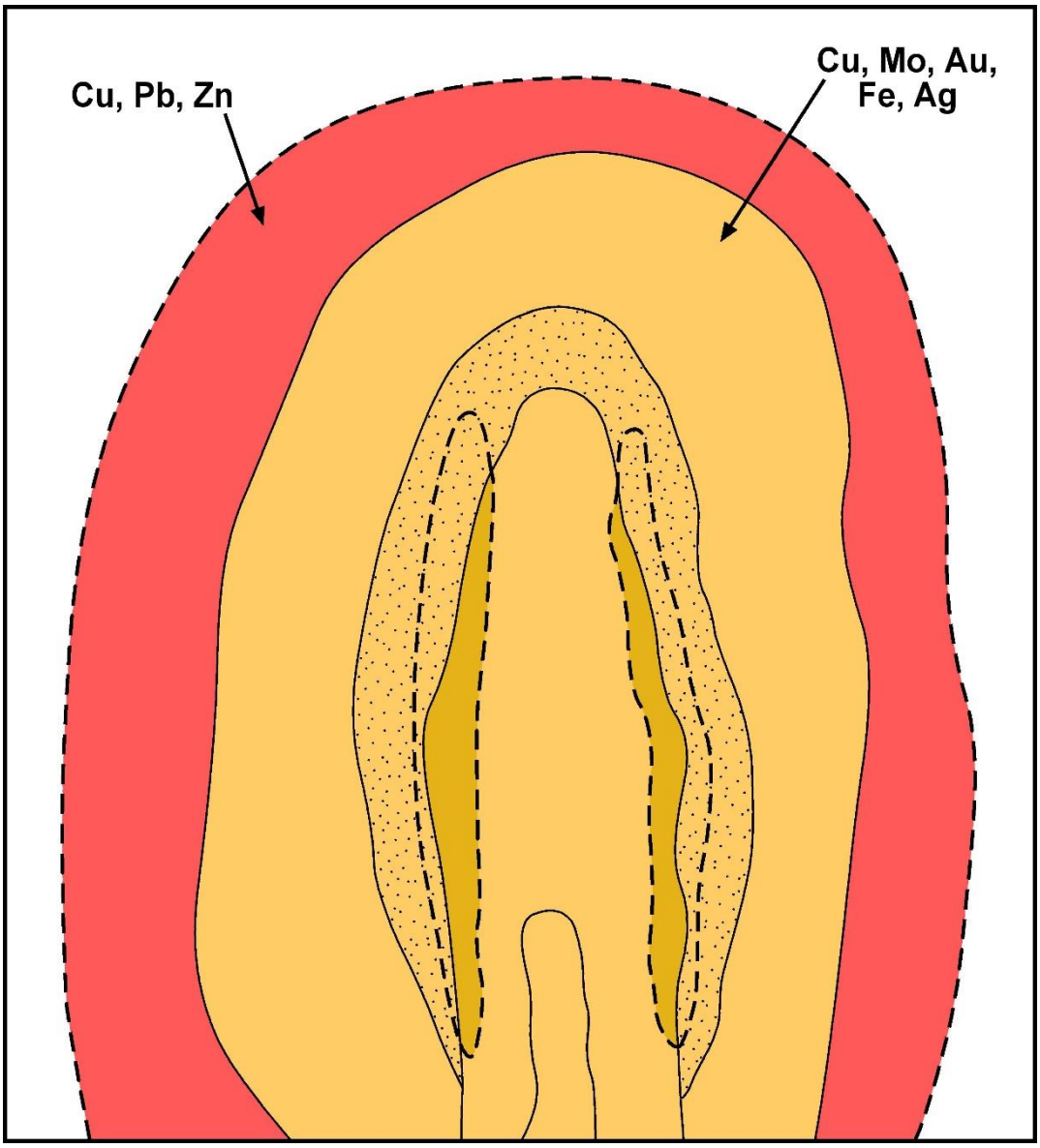

Figure 3: Schematic profile of an idealized magmatic-hydrothermal porphyry system and zones of metal mineralization (modified from Lowell & Gilbert, 1970).

Lead and Zinc Transportation and Deposition

Lead and zinc complex with chloride ($PbCl_2$ and $ZnCl_2$) in hydrothermal ore fluids and require reduced sulfur (H_2S) for the metals to precipitate as sulfide minerals (Holland, 1972; Burnham, 1979; Candela & Holland, 1984; Frank et al., 2002, 2011). Equilibria relating the transport of lead and zinc as chloride complexes and the formation of sulfide minerals in the porphyry, skarn, and MVT environments can be written as:

$$PbCl_2 + H_2S = PbS + 2\ HCl \quad (1)$$

and

$$ZnCl_2 + H_2S = ZnS + 2\ HCl, \quad (2)$$

(Anderson & Macqueen, 1982). The equilibria suggest that HCl and H_2S are the critical controlling factors in the transport and deposition of galena and sphalerite in porphyries, skarns, and MVT deposits. However, the relative importance of sulfur, chloride, and hydrogen chloride (HCl) in controlling the concentration and precipitation of lead and zinc are not well established.

High salinity magmatic brines are common in porphyry deposits and high chloride concentrations allow for substantial transportation of lead and zinc complexes prior to the precipitation of sulfide minerals in the peripheral of the deposit. Lead and zinc differ from the main copper deposit of the porphyry, not only by the location of the mineralization, but also by solubility of the other metals. Copper, gold, and iron also complex with chloride and precipitate closer to the causative intrusion than lead and zinc because they are less soluble in the fluid at lower temperatures (e.g. Candela & Holland, 1984; Pokrovski et al., 2005, 2013; Frank et al., 2011) The highest grade of lead and zinc in porphyry systems are often hosted by carbonate rocks (Sillitoe, 2010) since the reactive carbonate rock may have caused a rapid shift in pH to higher values, dropping the solubility of lead and zinc in solution, and producing mineralization

in relatively small volumes of rock (Hemley & Hunt, 1992). The absence of country rock that can neutralize effectively the HCl content of the hydrothermal fluid often results in lead and zinc mineralization being disseminated and, thus, sub-economic (Sillitoe, 2010).

MVT deposits form at much lower temperatures than porphyry deposits and are not sourced directly from a magma. They are similar in that a hydrothermal fluid transports lead and zinc before undergoing a physiochemical change that induces precipitation of galena and sphalerite. Sverjensky (1981) outlined three genetic models that may be responsible for precipitation of lead and zinc in MVT deposits: the mixing model, sulfate reduction model, and the reduced-sulfur model. It is likely that one or more of these proposed end-member models operate in each deposit.

The mixing model suggested the base metals were transported in a fluid that contained no significant amount of reduced sulfur. This means reduced sulfur was added to the metal-rich fluid by mixing with a fluid that contained H_2S or through thermal degradation of organic compounds in shales releasing sulfur (Sverjensky, 1981). Therefore, the precipitation of metal sulfides occurred when the metal-rich fluid interacted with the reduced sulfur. For example, if separate fluids, one metal-rich and the other H_2S-rich, converge at a site of deposition, this may be capable of generating large concentration gradients, high degree of saturation, and subsequent relatively rapid precipitation of sulfides.

The sulfate reduction model proposed the lead and zinc were transported with sulfate (SO_4^{2-}) in the ore fluid and then reduced for sulfide mineralization (Sverjensky, 1981). Reducing the sulfur already contained in a metal-bearing fluid at the site of ore deposition is judged more likely than the mixing of two separate fluids. If the sulfate reduction was produced locally then

there should be evidence such as the presence of gypsum or anhydrite, as well as a reducing agent like organic material (Anderson & Macqueen, 1982).

In the reduced-sulfur model, the base metals were transported in the fluid together with the reduced sulfur. The precipitation of galena and sphalerite occurred when the fluid is neutralized (increasing the pH of the fluid) by a reaction with the host rock (i.e. limestone). The generally accept pH for MVT fluids is between 3.5 and 4.5 (Hanor, 1994, 1996) which may be reactive enough with the carbonate host rock to cause precipitation. However, a recent fluid inclusion study from Kenderes and Appold (2016) showed the ore fluid may have a pH less than 2 based on the calcium concentration of the fluid assuming saturation with respect to fluorite. The reaction of an acidic fluid with carbonate will increase the pH (decrease HCl) and drive mineralization due to a drop in the solubility of metals in the ore fluid (Hemley & Hunt, 1992). Therefore, data on the capacity for a hydrothermal fluid to carry lead and zinc as a function of HCl and temperature is needed to constrain the formation of lead and zinc bearing porphyry and MVT deposits.

Previous Work

Very little research addresses the solubility of lead and zinc in hydrothermal fluids over a range of sulfur fugacity and acidity. A study by Hemley et al. (1992) and then subsequently expanded upon by Hemley and Hunt (1992) evaluated the concentrations of iron, lead, zinc, and copper in chloride solutions and with pH buffered by a quartz monzonite and the potassium feldspar-muscovite-quartz mineral assemblage. Experiments were performed at pressures of 50 to 200 MPa and at temperatures between 300 to 700°C. Lead and zinc concentrations were most strongly correlated to acidity, total chloride, temperature, and pressure. The solubilities for lead

and zinc were found to increase with increasing temperature and decrease with increasing pressure (Hemley et al., 1992). Acidity seemed to have the greatest impact on lead and zinc solubility whereas total chloride was a secondary control. The more HCl and chloride present in solution the higher the concentration of metals that fluid is capable of transporting (Pokrovski et al., 2005).

Hemley et al. (1992) is one of the only studies the focused on the solubility of lead and zinc in hydrothermal fluids; however, there is a dearth of data on their effects over a range of acidity in the porphyry and skarn systems and at temperatures typical of MVT mineralization. For this thesis work, the solubility of lead and zinc will be evaluated in hydrothermal fluids as a function of the HCl concentration of the fluid. Equilibria (1) and (2) suggest that HCl and H_2S are the critical controlling factors in the transport of $PbCl_2$ and $ZnCl_2$ and the deposition of galena and sphalerite. I hypothesize that these equilibria accurately describe the transport and precipitation of lead and zinc in most ore deposits and that, based on the equilibria, HCl exercises a major control on the solubility of lead and zinc and the subsequent precipitation of galena and sphalerite. High H_2S/HCl values are hypothesized to promote the formation of PbS or ZnS, whereas low values promote the dissolution of PbS or ZnS. The hypothesis was tested by performing experiments with variable HCl concentrations from 100 to 500°C and at a fixed pressure, sulfur fugacity, and total salinity. From these experiments, we determined the solubility of lead and zinc as a function of HCl and determine the relative efficiency of fluid neutralization as a precipitation mechanism. Solubility data on important base metals as a function of HCl concentration will be obtained and be cast in terms of equilibrium constants that can be used to predict mineral deposition.

CHAPTER II

Experimental and Analytical Techniques

Experimental Design

Experiments were conducted in René 41, Ni-based superalloy, cold-seal pressure vessels and placed in solid-state tube furnaces. The tube furnaces were heated with doubly wound Kanthal windings with each winding controlled separately to minimize the temperature gradient across the capsule. The temperatures of the experimental capsules were monitored with type-K (Chromel-Alumel) thermocouples inserted into external boreholes near the tip of the pressure vessels at the midpoint of the capsules (Figure 4). Previously, the temperature within the borehole was calibrated to within ±2°C from an internal thermocouple placed at the position of the capsules. Pressure was generated by a Haskel pump (model: DSHF-302) using water as the pressure medium. The pressure was monitored with an Astragauge pressure gauge calibrated within ±1 MPa by the manufacturer. Completed experimental runs were quenched from a run temperature to 200°C by using a stream of compressed air and then quick quenched in a water bath to room temperature before the capsules were removed.

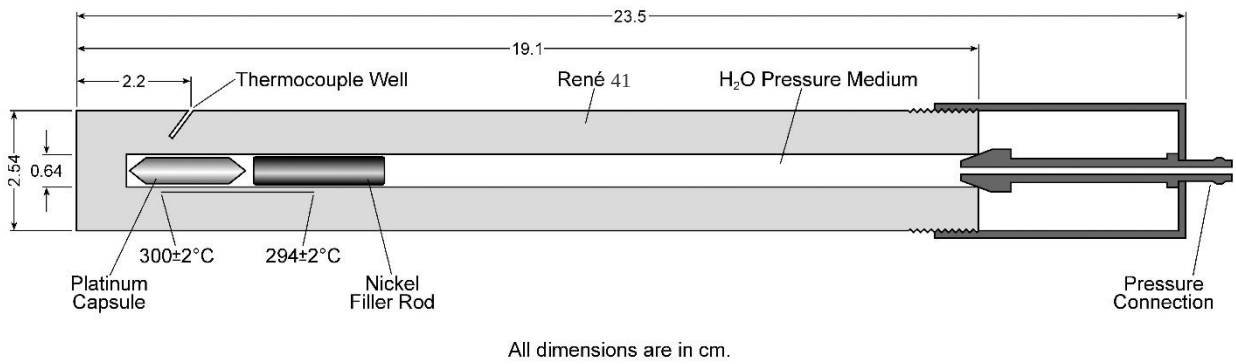

Figure 4: A diagram of the pressure vessel, position of the platinum capsule, nickel filler rod, and thermocouple borehole. All dimensions are in cm. The thermal gradient at the hot spot of the vessel and across the experimental charge is illustrated with temperature uncertainties (1 σ).

Starting Material

Experiments were performed in platinum (Pt) capsules, 1.5 to 3.0 mm long, created from Pt tubing with an outer diameter of 5.0 mm and wall thickness of 0.197 mm. The Pt tubing was 99.998% pure and purchased from Johnson Matthey. Capsules were loaded with (1) different combinations of natural sphalerite, galena, and Brazilian inclusion-free quartz with masses between 15 to 40 mg and (2) 20 to 70 µL of a HCl-NaCl aqueous fluid. Sphalerite and galena were natural hand samples purchased from Ward's Natural Science and the Brazilian inclusion-free quartz was donated by the Harvard Mineralogical Museum (Table 1).

Table 1: Experimental starting material compositions and source locations. Suppliers are listed for synthetic items and source locality for natural minerals. Starting compositions of all natural sulfide starting materials are an average of at least five JEOL JSM-5610LV scanning electron microscope spot analyses. The instrument automatically sums total weight percents to 100.

Starting Materials							
Material	**Company/Source Location**	**Composition/Purity**					
Natural Minerals		SiO_2 wt.%	Zn wt.%	Pb wt. %	S wt.%	Fe wt.%	Total wt.%
Galena	Reynolds County, MO, USA	-	-	88.08±0.78	11.92±0.78	-	100
Sphalerite	Santander, Spain	-	70.3±1.25	-	29.65±1.25	0.04±0.07	100
Quartz	Brazil	100	-	-	-	-	100
Synthetic Items							
Sodium Chloride	Fisher Scientific	99.98% NaCl					
Hydrochloric Acid	Fisher Scientific	~37.00% HCl					
Platinum	Johnson Matthey	99.95% Pt					
Nickel Rod	Alfa Aesar	99.90% Ni					

All other uncertainties (1 σ) are standard deviation from the mean.

Sphalerite and galena starting materials were crushed with a mortar and pestle and subsequently examined with a binocular microscope to remove visible impurities. The sphalerite and pre-crushed Brazilian inclusion-free quartz were fractured prior to loading for the purpose of capturing fluid inclusions. This was done by heating the minerals to 350°C in a Thermolyne Furnace 48000 for one hour followed by submersion in room-temperature deionized water. The samples were then dried in the oven and examined for fractures. The fluid inclusions in sphalerite and quartz were not analyzed for this study, but are available for future studies.

The HCl-NaCl-H_2O fluid had a bulk salinity of 15 wt.% $NaCl_{eq.}$. The chloride content of the fluid was split by moles between NaCl and HCl with a molar ratio varying between different experiments. The pH of the fluid in each experimental run was set by of the amount of HCl added. The pH of the remaining, unused aqueous fluid was measured using an Oakton pH/mV/Ion/°C meter to confirm the correct amount of HCl was added.

Loaded platinum capsules were crimped closed and subsequently welded with a Lampert PUK-3 professional welder (Figure 5). Capsule mass was checked at each step and any loss of mass attributed to volatilization of the aqueous fluid during sealing, reduced the reliability of the capsules. Any finished capsules with a total fluid mass loss greater than 5% were deemed a failure and discarded.

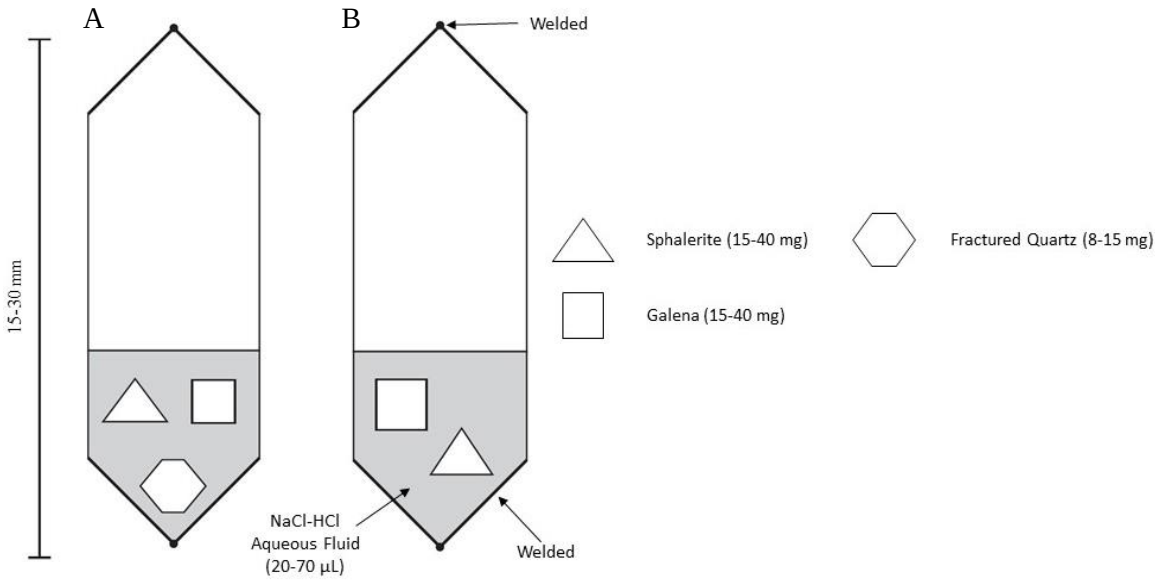

Figure 5: Different experimental capsules with dimensions and contents. A) Fractured quartz was added to the capsule for fluid inclusion. B) Standard capsule with only galena and sphalerite.

Experimental Conditions

Experiments were performed at 200, 300, or 500°C and 100 MPa. The fluid was equilibrated with galena and sphalerite for minimum run durations of 14 days at 500°C and 173 days for the lower temperature experiments where reaction kinetics were slower. The NaCl-HCl-H_2O fluid in all experiments fall within the supercritical fluid (Pitzer et al., 1984; Anderko & Pitzer, 1993; Bodner et al., 1985). A supercritical fluid exists at a pressure greater than the critical pressure for a given temperature.

Analytical Preparation and Technique

Platinum capsules were removed from the vessels after quench and subsequently cleaned, weighed, and visually inspected for leaks. Any capsule with a total fluid mass loss greater than 5% was judged to be a failure and discarded. The capsule was pierced with a hypodermic needle to draw out the experimental fluid. All punctured capsules emitted a gas with a strong odor of H_2S. The extracted fluid was injected into a glass vial with 2 to 7 mL of deionized water. All solid run products were subsequently removed from the capsules, washed with deionized water and stored in a glass vial for later compositional analyses.

Starting materials and sphalerite and galena run products were mounted into 1-inch mounts using Buehler 2 epoxide resin and Buehler EpoxiCure® 2 epoxy hardener, (mixed 4 to 1 parts by weight, respectively). The mounts were then polished with 400 and 600 grit Buehler silicon carbide powder to expose the interiors of all sulfide grains. Buehler 1.0 and 0.3 micron alpha alumina micropolish were used successively to create a smooth surface for analyses by a JEOL JSM-5610LV scanning electron microscope with energy dispersive spectroscopy (SEM-EDS).

All SEM mounts were sputter coated for 120 seconds with gold and palladium using a Polaron SEM Coating System. Representative proportions of galena and sphalerite grains from each run experiment were analyzed for lead, zinc, and sulfur by using EDS. The accelerating voltage of the electron beam was set to 20 kV with a spot size ranging from 40 to 300 μm. The relative compositions of sphalerite and galena grains from each experiment were measured and recorded to establish the equilibrium sulfide mineral assemblage.

The lead and zinc concentrations of the experimental fluid from experiments one through six where determined using a Perkin-Elmer model 3110 Atomic Absorption (AA) Spectrometer with an air–acetylene flame. Lead and zinc lamps, wavelengths of 217 nm and 213 nm, respectively, were used with currents between 10 to 15 mA with a silt of 0.7 nm and an integration time of one second. The Wisconsin State Laboratory of Hygiene at the University of Wisconsin-Madison analyzed the rest of the experimental fluid samples by using a Perkin-Elmer 5300 Dual-View Inductively Coupled Plasma Optical Emission Spectrometer (ICP-OES). The reported concentration, limit of detection (LOD), and limit of quantitation (LOQ) values have been adjusted for their own analytical dilutions and percent moisture where applicable.

Determination of Equilibrium Constants

Equilibrium constants for equations (1) and (2) at each temperature are defined as:

$$K(T,P) = \frac{f_{H_2S}^{sys} \times a_{PbCl_2}^{fluid}}{\left(a_{HCl}^{fluid}\right)^2 \times a_{PbS}^{Galena}} \quad (3)$$

and

$$K(T,P) = \frac{f_{H_2S}^{sys} \times a_{ZnCl_2}^{fluid}}{\left(a_{HCl}^{fluid}\right)^2 \times a_{ZnS}^{Sphalerite}} \quad (4)$$

The lead and zinc concentration data, along with the determined mineral compositions, will be used over a range of HCl concentrations and temperature to ascertain the concentrations of metals that can be carried by a given hydrothermal fluid; this will also provide insight into possible precipitation mechanisms. For this calculation, the hydrogen sulfide fugacity ($f_{H_2S}^{sys}$) and the activities of HCl, $ZnCl_2$, and $PbCl_2$ in the fluid must be determined. The activities of PbS in

galena and ZnS in sphalerite are denoted as a_{PbS}^{Galena} and $a_{ZnS}^{Sphalerite}$, respectively, and are unity for pure phases.

The $f_{H_2S}^{sys}$ of the system for each experiment was calculated after the sulfur fugacity ($f_{S_2}^{sys}$) and hydrogen fugacity ($f_{H_2}^{sys}$) were determined. The equilibrium and equilibrium constant to describe the reaction are:

$$^1/_2\,S_2 + H_2 = H_2S \tag{5}$$

and

$$K\,(T,P) = \frac{f_{H_2S}^{sys}}{(f_{S_2}^{sys})^{0.5} * f_{H_2}^{sys}} \tag{6}$$

First, the $f_{H_2}^{sys}$ needed to be determined from each experiment; this was done by using the following equilibrium and equilibrium constant equations:

$$^1/_2\,O_2 + H_2 = H_2O \tag{7}$$

and

$$K\,(T,P) = \frac{X_{H_2O}}{(f_{O_2}^{sys})^{0.5} + f_{H_2}^{sys}} \tag{8}$$

The oxygen fugacity of the system ($f_{O_2}^{sys}$) was buffered at nickel-nickel oxide (Ni-NiO) by the Ni-based René 41 vessel. The temperature-oxygen fugacity relationship was accounted for by using the pressure corrected Ni-NiO fugacity equation:

$$f_{O_2}^{sys} = 9.36 - \frac{24930}{T} + 0.046\left(\frac{P-1}{T}\right) \tag{9}$$

from Huehner and Sato (1970). Temperature is T and in Kelvin whereas P is pressure in bars. The mole fraction (X) of water (H_2O) was calculated for every experiment. The equilibrium

constant was determined using the SUPCRTBL software from Indiana University-Bloomington. By rearranging the above equilibrium constant equation, $f_{H_2}^{sys}$ can be solved for with:

$$f_{H_2}^{sys} = \frac{X_{H_2O}}{(f_{O_2}^{sys})^{0.5} * K} \quad (10)$$

Barton and Toulmin (1966) established the sulfur fugacity of the Fe-Zn-S system using sphalerite, pyrite, pyrrhotite assemblage. The $f_{S_2}^{sys}$ of each experiment was estimated from the variation in the composition of sphalerite and the temperature of the experiments (Figure 6).

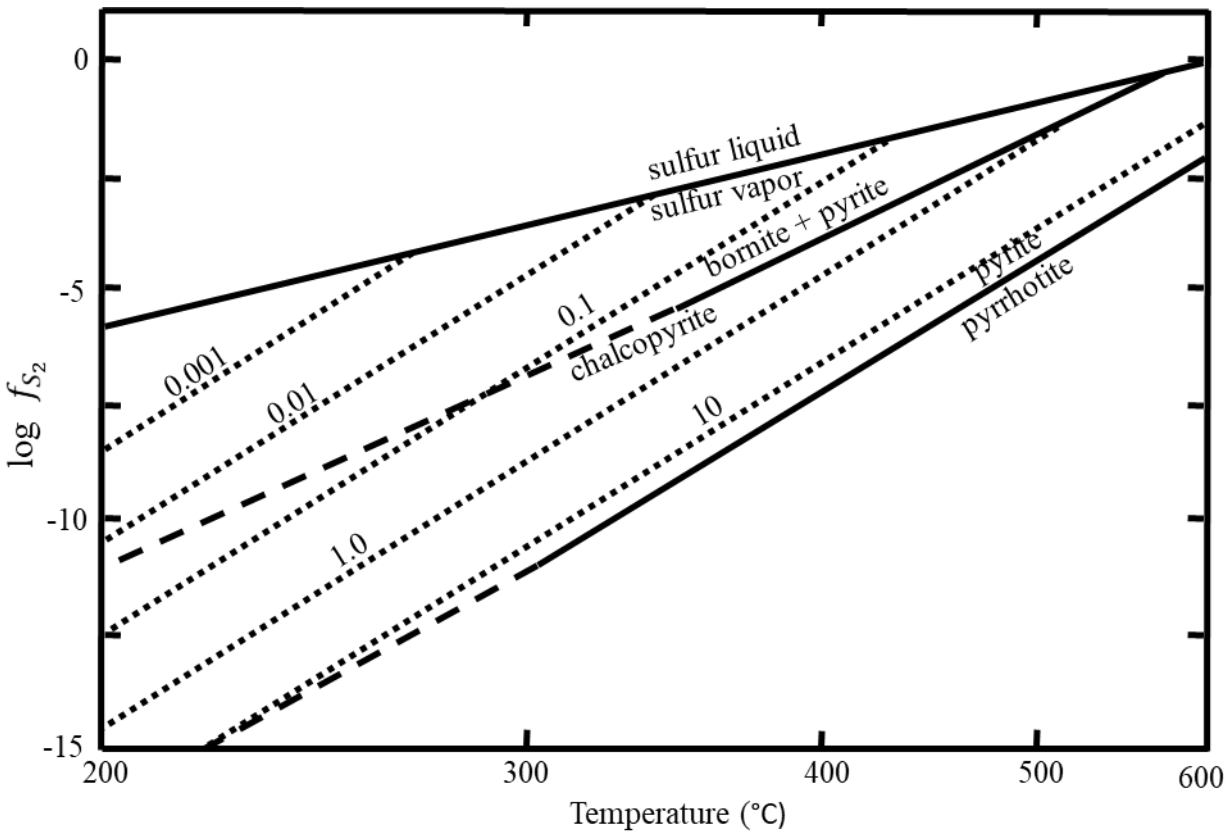

Figure 6: Sulfur fugacity versus temperature in portion of the Fe-Zn-S system. The dotted lines represent the variation in the composition of sphalerite (in mole percent FeS) in equilibrium with iron, pyrrhotite, or pyrite (modified from Barton & Toulmin, 1966).

The calculated $logf_{S_2}^{sys}$ ranged from log(-1) to log(-7.5) over the experimental temperature range. The $f_{S_2}^{sys}$ was then used along with the $f_{H_2}^{sys}$ and the equilibrium constant obtained from SUPCRTBL to calculate the f_{H_2S} of the systems through:

$$f_{H_2S}^{sys} = f_{H_2}^{sys} * (f_{S_2}^{sys})^{0.5} \quad (11)$$

The mole fractions of HCl, $PbCl_2$, and $ZnCl_2$ in the fluid and PbS and ZnS in galena and sphalerite were determined. The mole fractions are assumed to represent the activities of these components, or, in other words, the activity coefficients were assumed to be unity. It is common to assume activity coefficients of unity for dilute solutions as there are few ions to result in non-ideal behavior. Therefore, all mole fractions calculated equaled the activity.

The galena and sphalerite equilibrium constants for every experiment was calculated after all terms were defined.

Uncertainties

The glassware used for all dilutions were performed in Class A volumetric flasks that have an understood uncertainty of ± 0.1 mL. The Fisherbrand™ Finnpipette™ II adjustable-volume pipetters of 100 and 1000 µL were used for all small fluid measurements and have measurement uncertainties or ±0.4% and ±0.3%, respectively.

Uncertainties from the AA analyses may arise from an unstable flame which increases uncertainty due to fluctuations. A major problem arose when the AA fluid intake valve broke which affected at least the last analysis using the AA. The standard deviation for the absorbance of the standards for lead and zinc were 0.002 to 0.008 and 0.003 to 0.04, respectively.

The ICP-OES instrumental error was evaluated every ten samples to ensure the uncertainty was within ± 10%. Duplicate analysis for each sample were within 10% RPD (relative percent difference). There were experiments with metal concentration values above the limit of detection (LOD) which may factor into a higher uncertainty. Multiple concentrations at the same experimental condition were averaged and have a standard deviation within one sigma (1 σ).

The elemental concentration data from the SEM analyses had uncertainties distributed throughout the sulfides and were calculated from the standard deviation from the mean and reported as 1 σ.

CHAPTER III

RESULTS

Demonstration of Equilibrium

The concentrations of lead and zinc in synthetic hydrothermal fluids at experimental conditions similar to low-temperature MVT deposits and high-temperature porphyry deposits were determined in this study. Multiple experiments at 500°C and a HCl concentration of $5.35x10^4$ µg/g (Table 2) were conducted to assess if equilibrium had been reached. Equilibrium was evaluated with respect to time and fluid composition by noting the metal concentration at a given HCl concentration as a function of time. Lead concentrations at 500°C were broadly consistent at the HCl concentration of $5.35x10^4$ µg/g indicating equilibrium was reached after 14 days (Figure 7). There were not sufficient data to evaluate the equilibrium of lead or zinc solubility at other experimental conditions, but run times were considered to be appropriate to reach equilibrium based on the results at 500°C and from the previous study by Hemley et al. (1992) at lower temperatures.

Table 2: Lead concentrations for experiments of different durations to demonstrate equilibrium with respect to time. All experiments were conducted at 500°C and with the same starting materials.

Experiments with HCl of $5.35x10^4$ µg/g		
Experiment	Duration (Days)	Lead Concentration (µg/g)
E13C25	14	$6.6(\pm0.7)x10^3$
E13C24	18	$5.3(\pm0.5)x10^3$
E2C3*	29	$7.9(0.5)x10^3$
E1C2*	127	$4.8(0.5)x10^3$

Uncertainties are (1 σ) standard deviation from reported concentrations.
* Analyzed by AA

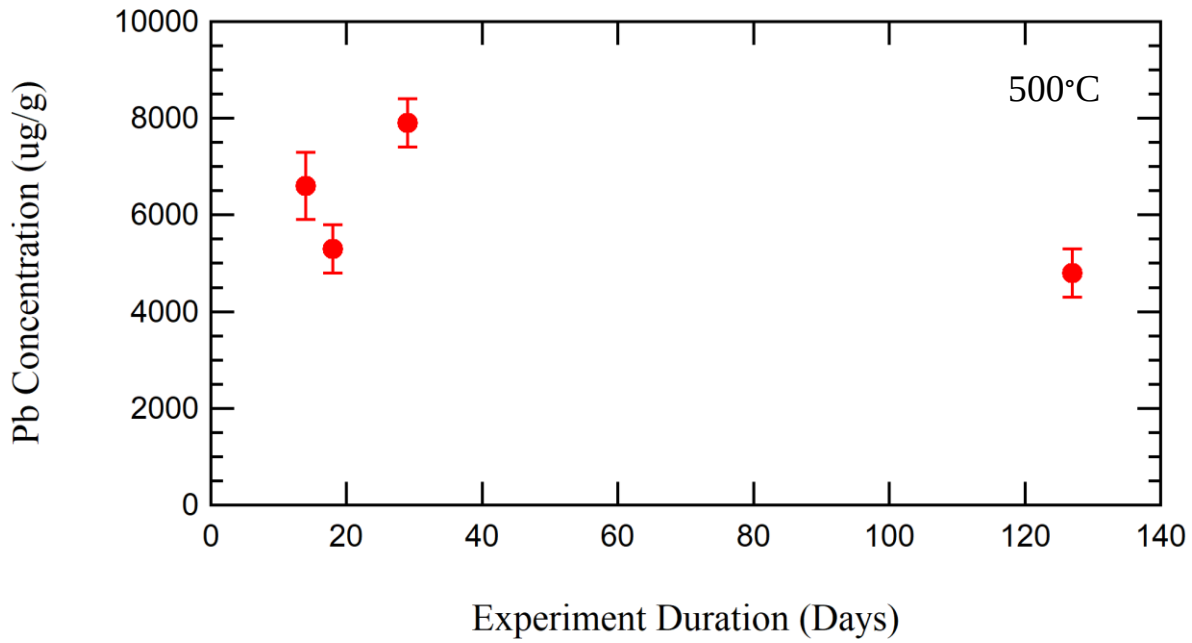

Figure 7: Lead concentration versus duration of experiment at 500°C and a HCl concentration of $5.35x10^4$ µg/g. Uncertainties are (1 σ) standard deviation of the experimental and analytical uncertainty.

Lead Concentrations in Experimental Fluids

The determined concentrations of lead in the synthetic hydrothermal fluids are listed in Table 3. Lead concentrations at 200°C ranged from $1.8x10^0$ to $1.1x10^1$ µg/g at HCl concentrations of $2.34x10^3$ µg/g and $9.35x10^3$ µg/g, respectively. The HCl concentrations at 300°C spanned from $3.17x10^2$ µg/g to $5.35x10^4$ µg/g with lead concentrations of $2.7x10^0$ µg/g and $1.6x10^1$ µg/g, respectively. Lead concentrations were determined in the fluid to be between $1.2x10^0$ µg/g and $7.9x10^3$ µg/g at 500°C and at HCl concentrations of $2.75x10^2$ µg/g to $5.35x10^4$ µg, respectively. Thus, lead concentrations were found to vary directly with temperature and the HCl concentration of the fluid (Figures 8A, 8B, 8C).

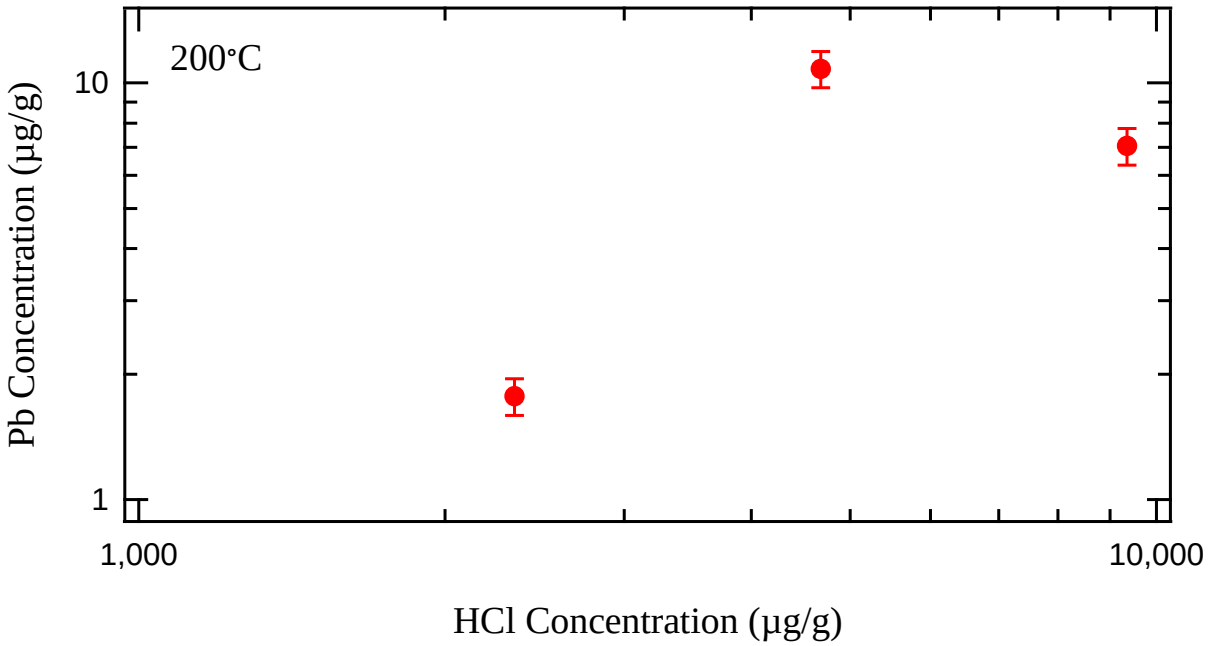

Figure 8A: Lead concentration versus HCl concentration of the experimental fluid for experiments at 200°C. The lead concentrations vary directly with the HCl concentrations of the fluid. Uncertainties are (1 σ) standard deviation of the experimental and analytical uncertainty.

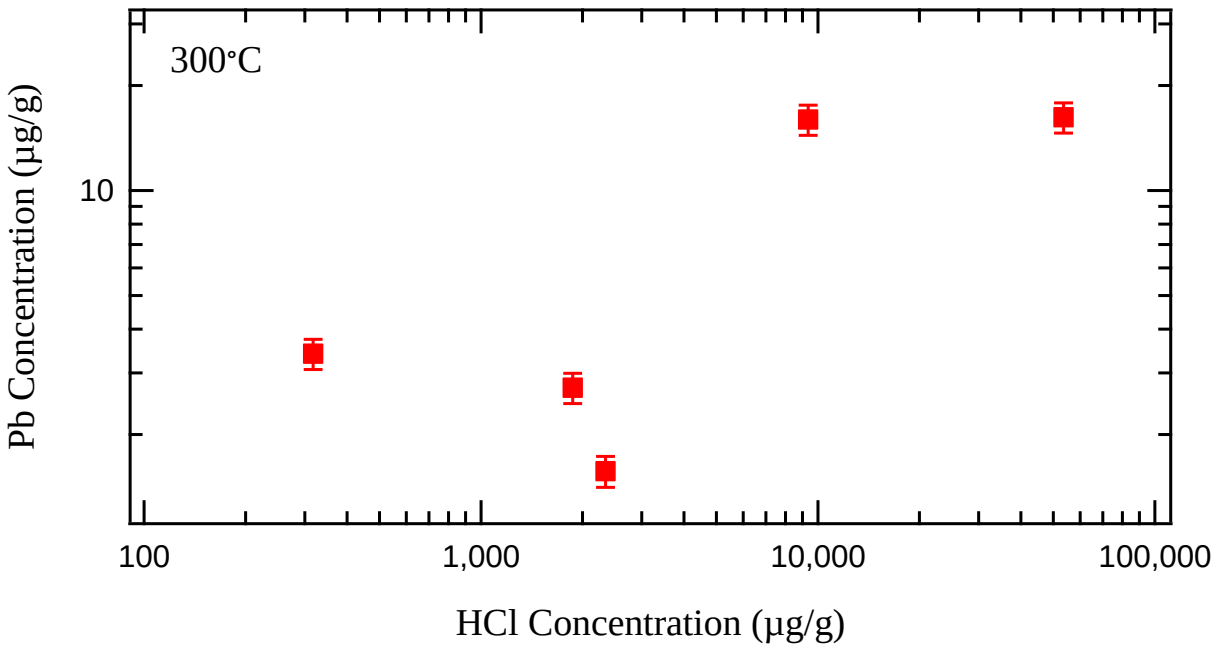

Figure 8B: Lead concentrations versus HCl concentration of the experimental fluid for the 300°C. The lead concentrations have a positive trend with the HCl concentrations. Uncertainties are (1 σ) standard deviation of the experimental and analytical uncertainty.

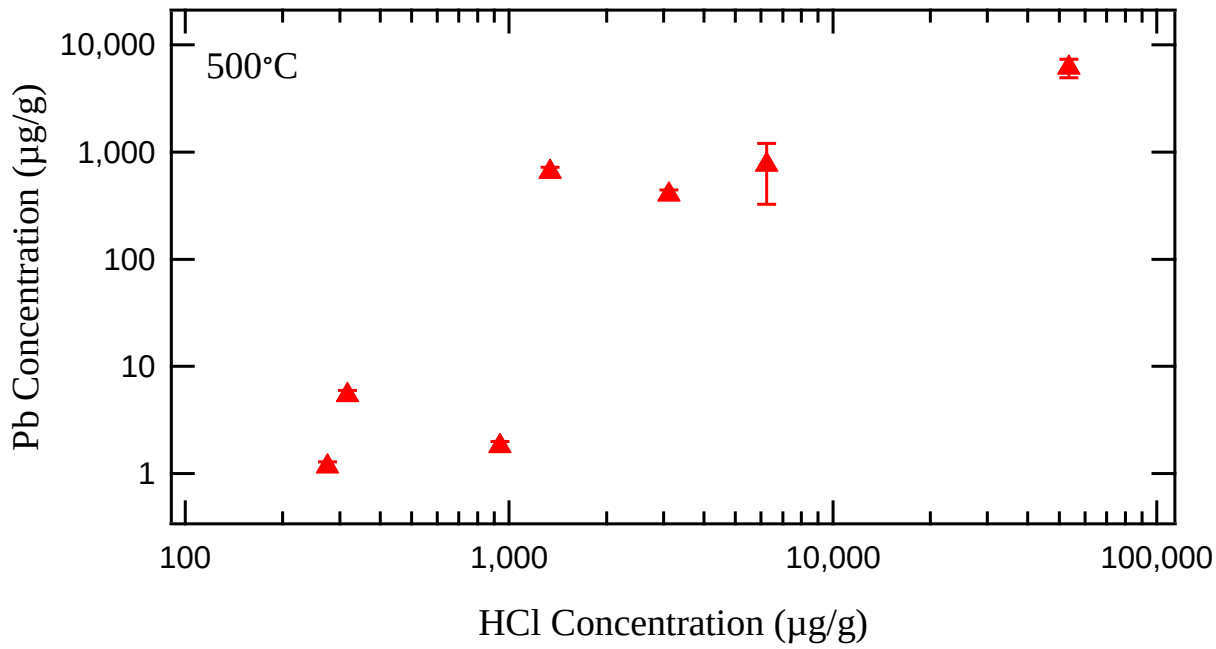

Figure 8C: Lead concentrations versus HCl concentration of the experimental fluid for the 500°C. The lead concentrations have a positive trend with the HCl concentrations. Uncertainties are (1 σ) standard deviation of the experimental and analytical uncertainty.

Table 3: Lead and zinc concentrations from AA and ICP-OES analyses for each experiment. The total salinity for all experiments was set at 15 wt.% $NaCl_{eq}$. To keep $NaCl_{eq.}$ concentrations at 15 wt.%, actual NaCl concentrations would decrease as HCl concentrations were increased.

Experiment	Temperature (°C)	Duration (Days)	NaCl wt.%	HCl (µg/g)	Pb (µg/g)	Zn (µg/g)
E12C23	200	113	13.64	$9.36x10^3$	$7.1(\pm0.7)x10^0$	$1.3(\pm0.1)x10^3$
E9C17	200	173	14.28	$4.68x10^3$	$1.1(\pm0.1)x10^1$	$5.5(\pm0.5)x10^2$
E11C21	200	113	14.63	$2.34x10^3$	$1.8(\pm0.2)x10^0$	$1.7(\pm0.2)x10^2$
E13C26	300	55	9.55	$5.35x10^4$	$1.6(\pm0.2)x10^1$	$1.2(\pm0.1)x10^3$
E2C4*	300	103	9.55	$5.35x10^4$	N.D.	$2.4(\pm0.3)x10^3$
E14C27	300	52	13.64	$9.36x10^3$	$1.6(\pm0.2)x10^1$	$4.1(\pm0.4)x10^2$
E14C28	300	52	13.64	$9.36x10^3$	B.D.	$2.8(\pm0.3)x10^3$
E11C22	300	113	14.63	$2.34x10^3$	$1.6(\pm0.2)10^0$	$4.5(\pm0.5)x10^2$
E7C14	300	31	14.71	$1.87x10^3$	$2.7(\pm0.3)x10^0$	$1.1(\pm0.1)x10^3$
E5C10	300	84	14.95	$3.17x10^2$	$3.4(\pm0.3)x10^0$	$2.4(\pm0.2)x10^2$
E1C2*	500	127	9.55	$5.35x10^4$	$4.8(\pm0.5)x10^3$	N.D.
E2C3*	500	29	9.55	$5.35x10^4$	$7.9(\pm0.5)x10^3$	N.D.
E13C24	500	18	9.55	$5.35x10^4$	$5.3(\pm0.5)x10^3$	$2.6(\pm0.3)x10^3$
E13C25	500	14	9.55	$5.35x10^4$	$6.6(\pm0.7)x10^3$	$1.8(\pm0.2)x10^3$
E3C6*	500	50	13.64	$9.36x10^3$	N.D.	$9.6(\pm0.2)x10^2$
E10C18	500	15	14.06	$6.24\ x10^3$	$3.3(\pm0.3)x10^2$	$5.5(\pm0.5)x10^2$
E10C20	500	42	14.06	$6.24\ x10^3$	$1.2(\pm0.1)x10^3$	$5.7(\pm0.6)x10^2$
E8C16	500	17	14.516	$3.12x10^3$	$4.0(\pm0.4)x10^2$	$1.7(\pm0.2)x10^3$
E15C29	500	18	14.79	$1.34x10^3$	$6.5(\pm0.7)x10^2$	$1.0(\pm0.1)x10^2$
E4C8	500	91	14.85	$9.36x10^2$	$1.8(\pm0.2)x10^0$	$1.7(\pm0.2)x10^2$
E5C11	500	89	14.95	$3.17x10^2$	$5.4(\pm0.5)x10^0$	$6.6(\pm0.7)x10^2$
E6C12	500	32	14.96	$2.75x10^2$	$1.2\pm(0.1)x10^0$	$2.0(\pm0.2)x10^2$

Uncertainties are (1 σ) standard deviation from reported concentrations

B.D. = below detection, N.D. = No data

* Analyzed by AA

Zinc Concentrations in Experimental Fluids

The concentration of zinc in the synthetic hydrothermal fluids are listed in Table 3. Experiments at 200°C were determined to have zinc concentration from $1.7x10^2$ µg/g to $1.7x10^3$ µg/g at HCl concentrations of $2.34x10^3$ µg/g and $9.36x10^3$, respectively. HCl concentration imposed in experiments at 300°C ranged from $3.17x10^2$ µg/g to $5.35x10^4$ µg/g and zinc concentrations were determined at those HCl concentrations to be $2.4x10^2$ µg/g and $2.8x10^3$ µg/g, respectively. At 500°C, HCl concentrations and zinc concentration ranged from $2.75x10^2$ µg/g to $5.35x10^4$ µg/g and $2.0x10^2$ µg/g to $2.6x10^3$ µg/g, respectively. The concentration of zinc in the synthetic hydrothermal fluids were found to increase directly with HCl concentrations (Figures 9A, 9B, 9C).

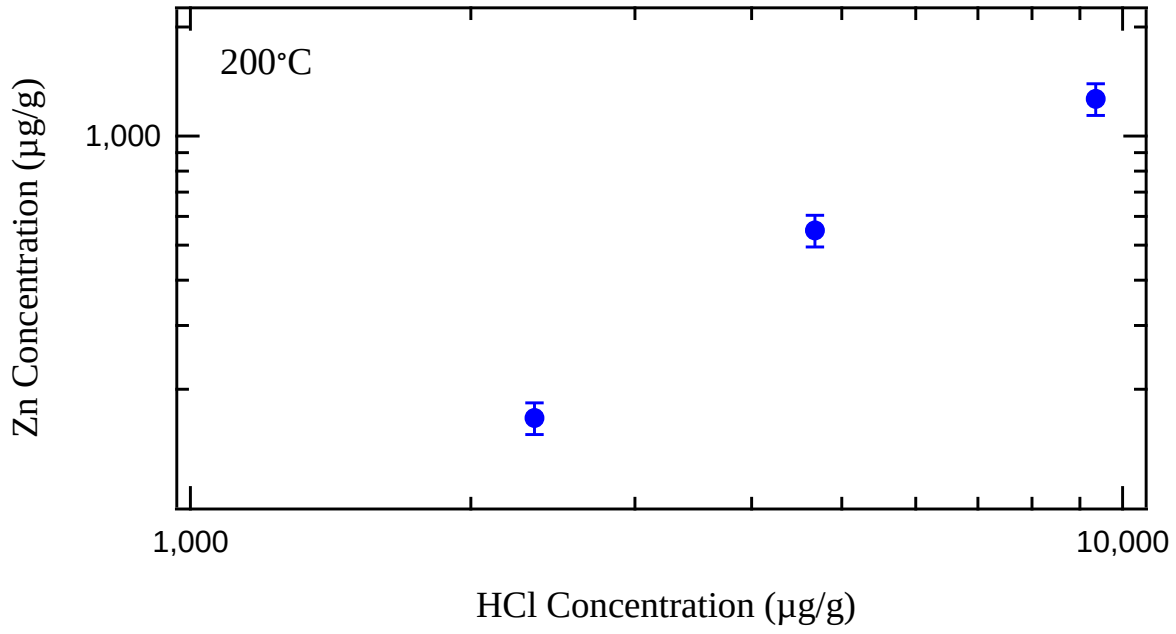

Figure 9A: Zinc concentrations versus HCl concentration of the experimental fluid for the 200°C. The zinc concentrations have a positive trend with the HCl concentrations. Uncertainties are (1 σ) standard deviation of the experimental and analytical uncertainty.

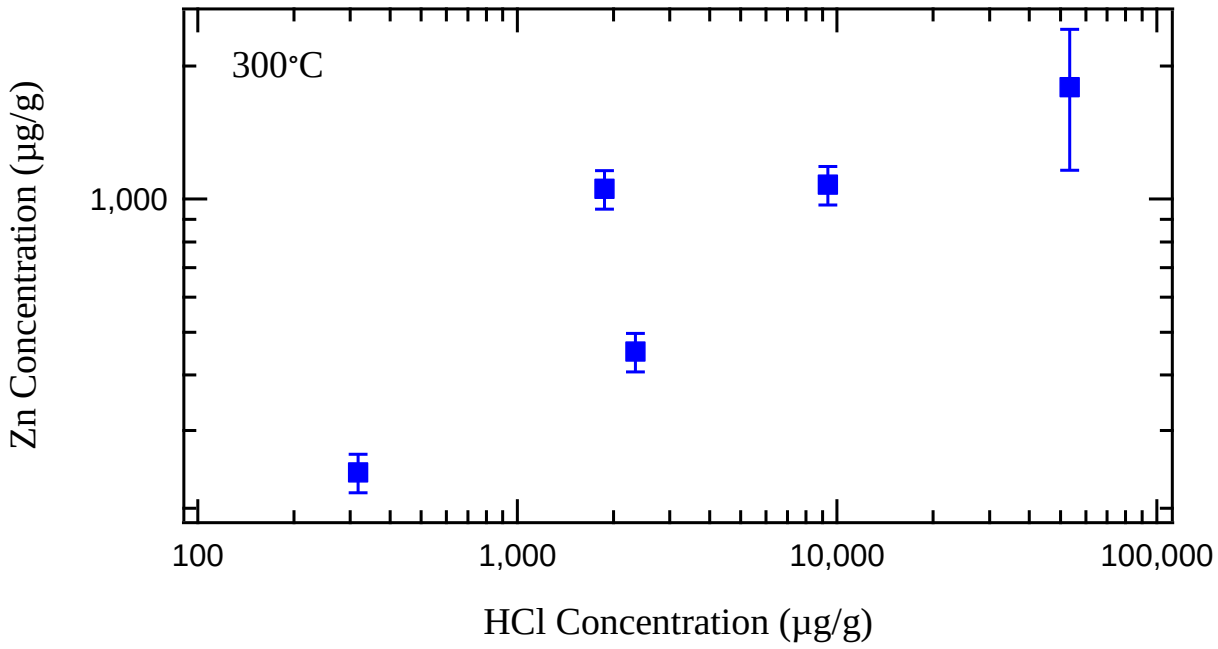

Figure 9B: Zinc concentrations versus HCl concentration of the experimental fluid for the 300°C. The zinc concentrations have a positive trend with the HCl concentrations. Uncertainties are (1 σ) standard deviation of the experimental and analytical uncertainty.

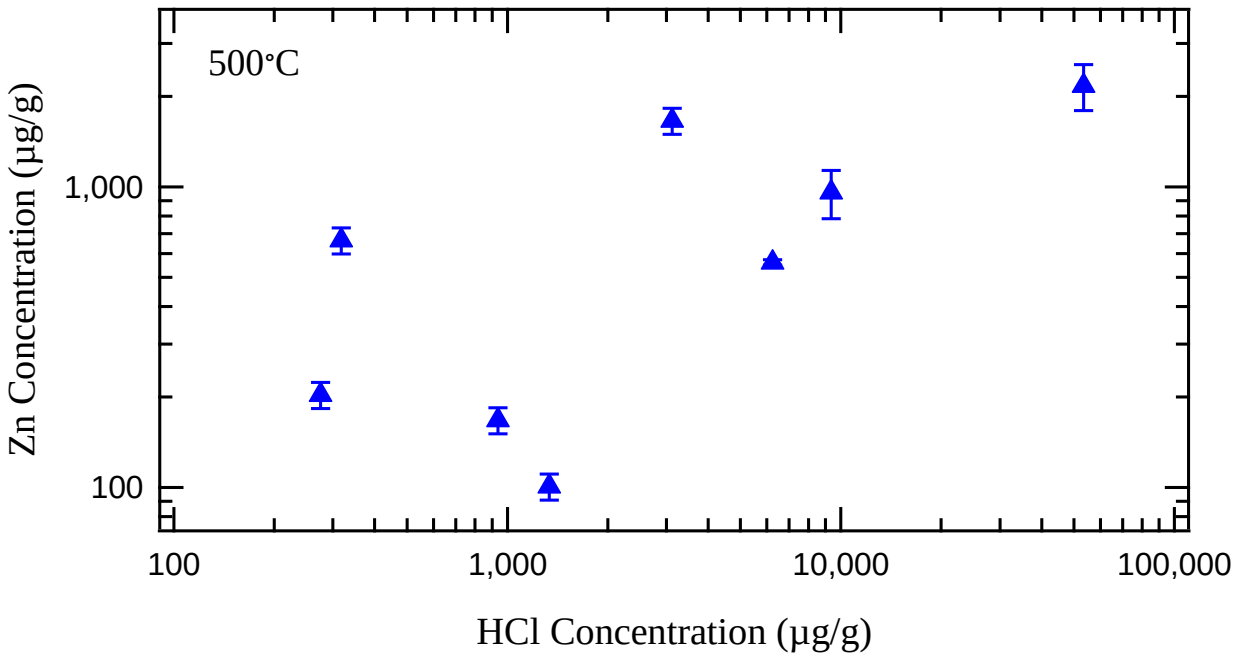

Figure 9C: Zinc concentrations versus HCl concentration of the experimental fluid for the 500°C. The zinc concentrations have a positive trend with the HCl concentrations. Uncertainties are (1 σ) standard deviation of the experimental and analytical uncertainty.

Major Element Concentrations in Sulfide Minerals

Major element concentrations of galena and sphalerite starting materials and run products were determined for all experiments (Appendix 1). Five to ten compositional points of the samples were taken and an average composition of each mineral grain was determined with uncertainties of 1 σ standard deviation from the mean. All compositional data summed to a 100 wt.%.

Sphalerite was either pure or very close to pure in the starting material and all experiments. Only 10 of the 22 successful experiments recorded anything but zinc and sulfur. Iron was the most common impurity and ranged from 0.05 to 0.16 wt.%. This impurity should not have an impact on the availability of zinc to dissolve into the fluid, but does affect slightly the activity of sphalerite in the equilibrium constant calculation. Natural samples of sphalerite are rarely pure and typically contain significant amounts of iron, cadmium, and manganese substituting for zinc, as well as small amounts of gallium, germanium, indium, cobalt, and mercury. The most common impurity is iron which can reach up to 15 wt.% (Cook et al., 2009). All galena starting materials and run products were found to be pure and only contained lead and sulfur.

Galena and Sphalerite Equilibrium Constants

Equilibrium constants for the equilibria (eq. 3 and 4) relating to the transport of lead and zinc as chloride complexes and the formation of sulfide minerals were calculated (Table 4). The equilibrium constants for equilibrium (3), $PbCl_2$/galena, at 200, 300, and 500°C were calculated as $2.01(\pm1.24)x10^4$, $5.12(\pm8.77)x10^4$, and $5.10(\pm7.67)x10^2$, respectively. Equilibrium constants

for equilibrium (4), $ZnCl_2$/sphalerite, were $8.46(\pm1.32)x10^4$, $5.23(\pm7.30)x10^4$, and $1.29(\pm1.96)x10^2$ at 200, 300, and 500°C, respectively. The large uncertainties in the average equilibrium constants at 300 and 500°C are the result of a select few outlying concentration data, all from the lowest HCl concentration experiments. Further, the concentration data from the 300°C experiments exhibited a negative trend with increasing HCl concentrations in the fluid. For any given temperature, the higher HCl concentration experiments have lower equilibrium constants increasing upward to the low HCl concentration experiments. This may be a result of experimental uncertainty, variance from the initial HCl concentration, or, less likely, misidentified equilibria.

Table 4: Calculated equilibrium constants for equation (3) and (4) of galena and sphalerite, respectively, at every experimental conditions. The total salinity for all experiments was set at 15 wt.% $NaCl_{eq}$.

Experiment	Temperature (°C)	Duration (Days)	$f_{H_2S}^{sys}$	a_{HCl}^{fluid}	$a_{PbCl_2}^{fluid}$	$a_{ZnCl_2}^{fluid}$	a_{PbS}^{Galena}	a_{ZnS}^{Sphal}	K_{Eq3}	K_{Eq4}
E12C23	200	113	$3.63x10^{1}$	$4.08x10^{-3}$	$1.25x10^{-11}$	$4.57x10^{-9}$	1.00	1.00	$3.67x10^{4}$	$1.00x10^{2}$
E9C17	200	173	$3.62x10^{1}$	$2.12x10^{-3}$	$1.76x10^{-11}$	$1.82x10^{-9}$	1.00	1.00	$7.05x10^{3}$	$6.80x10^{1}$
E11C21	200	113	$3.62x10^{1}$	$1.09x10^{-4}$	$1.99x10^{-12}$	$3.81x10^{-10}$	1.00	1.00	$1.64x10^{4}$	$8.55x10^{1}$
E13C26	300	55	$4.90x10^{1}$	$1.69x10^{-2}$	$2.58x10^{-11}$	$3.77x10^{-9}$	1.00	1.00	$2.26x10^{5}$	$1.55x10^{3}$
E2C4*	300	103	$4.90x10^{1}$	$1.69x10^{-2}$	N.D.	$3.27x10^{-9}$	1.00	1.00	N.C.	$1.78x10^{3}$
E14C27	300	52	$4.91x10^{1}$	$4.08x10^{-3}$	$2.42x10^{-11}$	$1.26x10^{-9}$	1.00	1.00	$1.40x10^{4}$	$2.68x10^{2}$
E14C28	300	52	$4.91x10^{1}$	$4.08x10^{-3}$	N.D.	$8.66x10^{-9}$	1.00	1.00	N.C.	$3.91x10^{1}$
E11C22	300	113	$4.90x10^{1}$	$1.09x10^{-3}$	$1.96x10^{-12}$	$1.15x10^{-9}$	1.00	1.00	$1.23x10^{4}$	$4.04x10^{1}$
E7C14	300	31	$4.90x10^{1}$	$8.66x10^{-4}$	$4.74x10^{-12}$	$3.75x10^{-9}$	1.00	0.99	$3.23x10^{3}$	$1.24x10^{0}$
E5C10	300	84	$4.90x10^{1}$	$1.49x10^{-4}$	$2.54x10^{-12}$	$3.66x10^{-10}$	1.00	1.00	$1.78x10^{2}$	$8.08x10^{0}$
E1C2*	500	127	$8.25x10^{1}$	$1.69x10^{-2}$	$1.26x10^{-9}$	N.D.	1.00	1.00	$2.75x10^{3}$	N.C.
E2C3*	500	29	$8.25x10^{1}$	$1.69x10^{-2}$	$5.64x10^{-9}$	N.D.	1.00	1.00	$6.14x10^{2}$	N.C.
E13C24	500	18	$8.26x10^{1}$	$1.69x10^{-2}$	$8.47x10^{-9}$	$8.30\ x10^{-9}$	1.00	1.00	$4.09x10^{2}$	$4.17x10^{2}$
E13C25	500	14	$8.27x10^{1}$	$1.69x10^{-2}$	$1.05\ x10^{-8}$	$5.83\ x10^{-9}$	1.00	1.00	$3.30x10^{2}$	$5.94x10^{2}$
E3C6*	500	50	$8.26x10^{1}$	$4.08x10^{-3}$	N.D.	$1.56\ x10^{-9}$	1.00	1.00	N.C.	$1.29x10^{2}$
E10C18	500	15	$8.26x10^{1}$	$2.79x10^{-3}$	$4.94x10^{-10}$	$1.69\ x10^{-9}$	1.00	1.00	$1.90x10^{2}$	$5.57x10^{1}$
E10C20	500	42	$8.25x10^{1}$	$2.79x10^{-3}$	$1.51x10^{-9}$	$1.47\ x10^{-9}$	1.00	1.00	$6.22x10^{1}$	$6.41x10^{1}$
E8C16	500	17	$8.25x10^{1}$	$1.43x10^{-3}$	$5.02x10^{-10}$	$4.23\ x10^{-9}$	1.00	1.00	$4.91x10^{1}$	$5.82x10^{0}$
E15C29	500	18	$8.25x10^{1}$	$6.27x10^{-4}$	$1.14x10^{-9}$	$3.58x10^{-10}$	1.00	1.00	$4.18x10^{0}$	$1.33x10^{1}$
E4C8	500	91	$8.25x10^{1}$	$4.37x10^{-4}$	$2.25x10^{-12}$	$4.25x10^{-10}$	1.00	1.00	$1.03x10^{3}$	$5.45x10^{0}$
E5C11	500	89	$8.25x10^{1}$	$1.49x10^{-4}$	$3.7\ x10^{-12}$	$9.41x10^{-10}$	1.00	1.00	$7.16x10^{1}$	$2.86x10^{-1}$
E6C12	500	32	$8.25x10^{1}$	$1.29x10^{-4}$	$2.04x10^{-12}$	$7.25x10^{-10}$	1.00	1.00	$9.09x10^{1}$	$2.78x10^{-1}$

N.D.= no data, N.C.= not calculated, data *= analyzed by AA

CHAPTER IV
DISCUSSION

Relationship of Experiments to Natural Systems

The compositions of the synthetic hydrothermal fluids were set to mimic natural hydrothermal fluids, but were simplified to limit the number of variables that can influence metal concentration. Natural hydrothermal fluids are dominated by NaCl, KCl, HCl, and H_2O, but may also contain CO_2, N_2, H_2S, SO_2, base metals, and precious metals, such as gold, in select porphyry systems (Catchpole et al., 2011; Heinrich, 2005). This study worked with chloride-rich and sulfide-saturated fluids as those components are the most abundant and thought to be the most important in lead- and zinc-bearing deposits.

The total salinity of the synthetic hydrothermal fluids were set at 15 wt.% $NaCl_{eq.}$ since it was a median salinity for both deposits. MVT deposits typically have salinities that vary from 10 to 25 wt.% NaCl with some studies finding as much as 30 wt.% NaCl (Appold & Wenz, 2011; Kesler et al., 1989; Pelch et al., 2015; Sverjensky, 1986). Hydrothermal fluids in porphyry deposits have a wide range of salinities and compositions; generally, the salinity of the fluid decreases with increasing distance from the causative igneous intrusion. Many fluid inclusions found spatially with lead-zinc veins are found to have salinities of 2 to 12 wt.% NaCl (Catchpole et al., 2011; Heinrich, 2005; Lawley et al., 2010; Sillitoe, 2010); however, the metal-rich brine that transported the metals from the magma to the site of deposition can have much higher values

of 35 to 60 wt.% NaCl (e.g. Allan et al., 2011; Hedenquist et al., 1998; Imer et al., 2016; Nash, 1967).

MVT and porphyry-style deposits are different in many ways, but they are similar in that lead and zinc are transported as chloride complexes, $PbCl_2$ and $ZnCl_2$, in hydrothermal fluids (Hemley, 1953; Anderson, 1973; Giordano & Barnes, 1979; Giordano and Barnes, 1981; Sverjensky, 1986; Hemley & Hunt, 1992; Heinrich et al., 1999; Catchpole et al., 2011). Since the minerals and metal complexes are the same in both systems, the same precipitation reactions are likely and, thus, changes in HCl or H_2S at any given temperature can induce the formation of galena and/or sphalerite (e.g. Sverjensky, 1981; Sillitoe, 2010). As is noted above, MVT and porphyry deposits are different in that MVT deposits occur at lower temperatures, 50 to 300°C, whereas porphyry deposits are at 200 to 600°C. This study used experimental parameters that attempted to match natural hydrothermal lead-zinc deposits as closely as possible, but also tried to limit multiple variables influencing metal concentration. The data from this study demonstrated that the concentrations of the lead and zinc in synthetic hydrothermal fluids increased directly with HCl concentration with only lead concentration experiencing a temperature effect.

Evaluation of Data and Equilibrium Constants

Equations (3) and (4) suggest that HCl is a critical controlling factor in the transportation of lead and zinc in a hydrothermal fluid and in the precipitation of galena and sphalerite. Low HCl values promote the formation of galena or sphalerite, whereas high values promote the dissolution of the minerals. Lead solubility was found to decrease significantly with declining HCl concentration, but also decreased with decreasing temperatures (Figure 10). Likewise, the

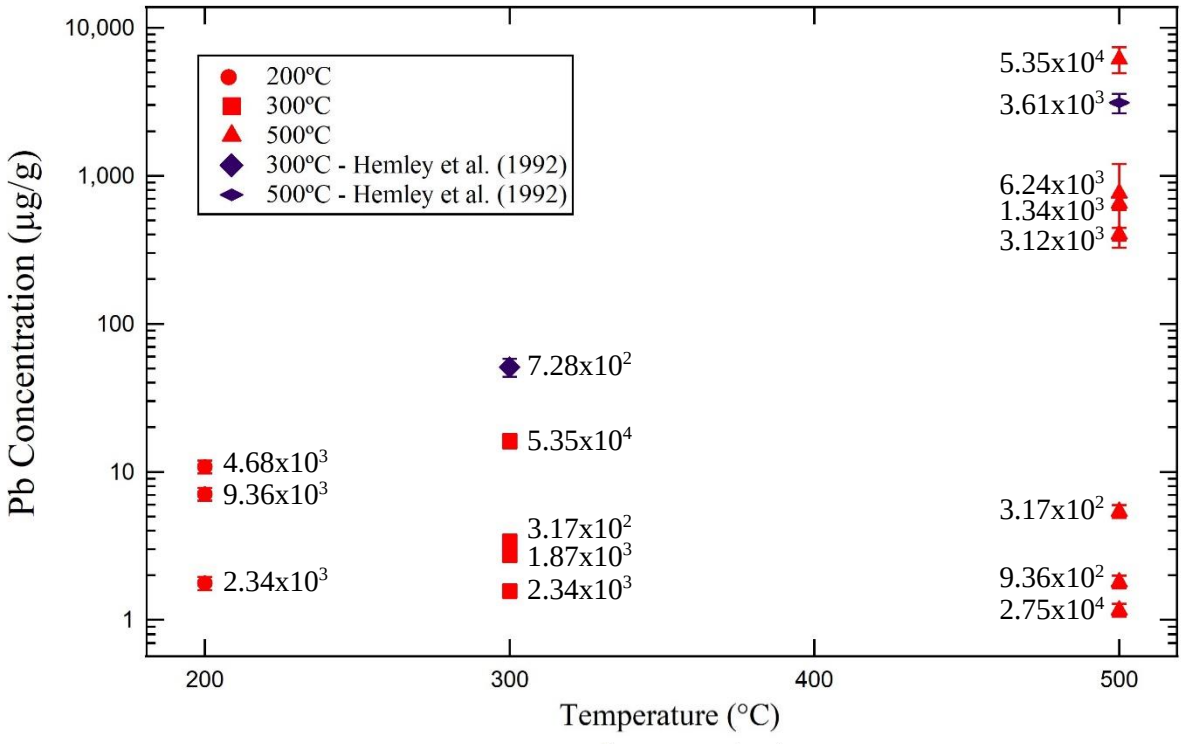

Figure 10: Lead concentrations over a range of HCl concentrations at 200, 300, and 500°C. Each point is labelled with the corresponding HCl concentration (µg/g) for that experiment. Data included from the Hemley et al. (1992) study. Uncertainties are (1 σ) standard deviation of the experimental and analytical uncertainty.

solubility of zinc decreased with HCl concentration, but temperature has less of an impact on the solubility and instead appears to be relatively constant over the temperature range (Figure 11). Decreasing HCl concentrations (increasing pH) would be efficient at inducing both galena and sphalerite precipitation (Figures 10, 11 & 14). The variable lead to zinc ratios observed in some ore-bearing systems may be the result of differences in the rate of change of temperature and acidity which drive the precipitation of galena and sphalerite in MVT and porphyry systems. However, decreasing temperature would appear to be more effective at inducing precipitation of galena than sphalerite.

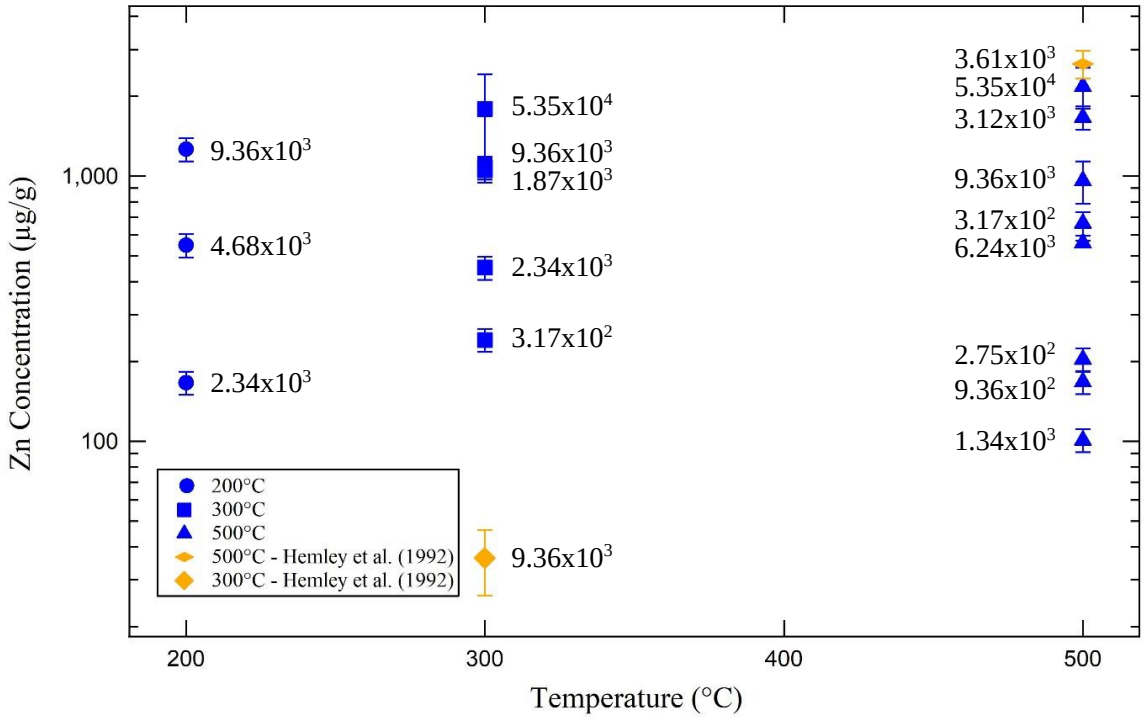

Figure 11: Zinc concentrations over a range of HCl concentrations at 200, 300, and 500°C. Each point is labelled with the corresponding HCl concentration (µg/g) for that experiment. Data included from the Hemley et al. (1992) study. Uncertainties are (1 σ) standard deviation of the experimental and analytical uncertainty.

The equilibrium constants are broadly consistent, but there are minor variations in regards to the lowest HCl concentration experiments. To evaluate the equilibrium constants, the average equilibrium constants for equilibriums (3) and (4) at every temperature were used to calculate the concentrations of lead and zinc from each experiment. The experimental concentrations were plotted versus the calculated concentrations to examine any deviation between the two values (Figure 12). The low HCl experiments for zinc and lead at 300 and 500°C experiment are the least similar to model calculated values. This inconsistency of the low HCl equilibrium constants between experiments at the same temperature may have resulted from a lack of HCl in the system. The HCl may have become a limiting reagent in the chemical reaction causing the experiments to not reach equilibrium.

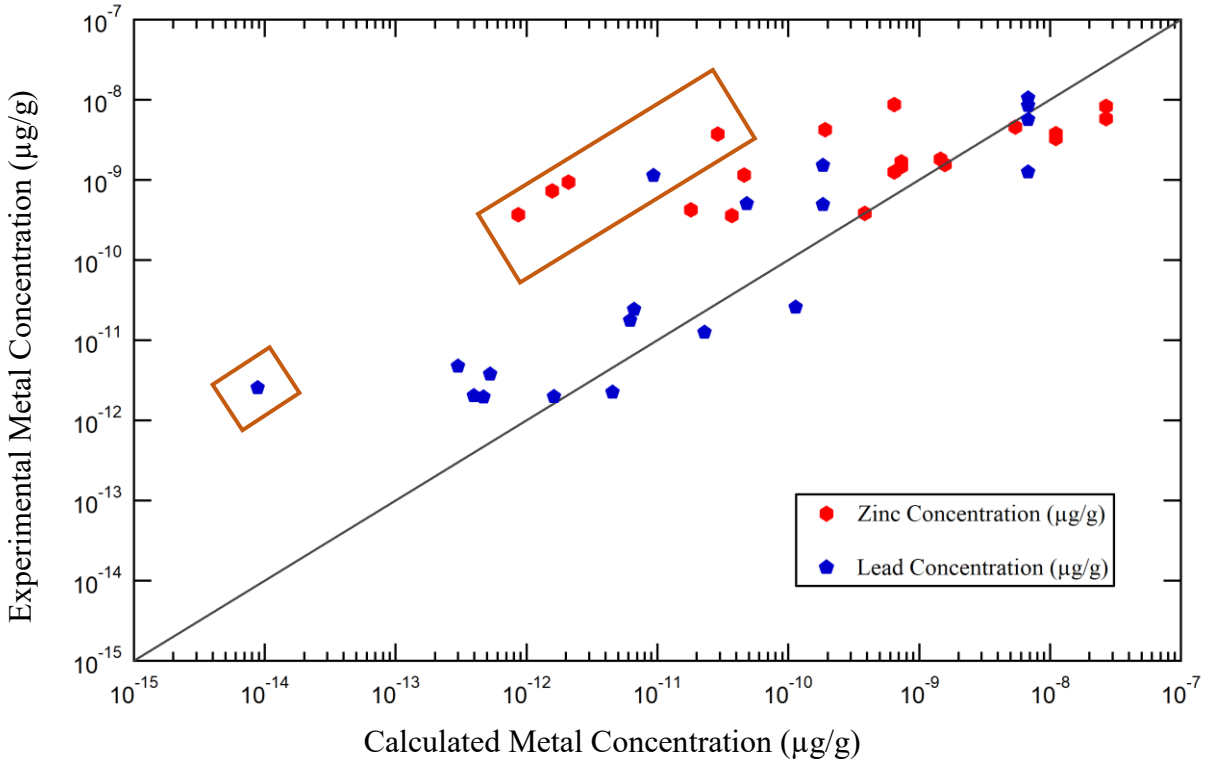

Figure 12: Experimental metal concentrations versus calculated metal concentrations. The gray line represents where $C_{Metal}^{Experimental} = C_{Metal}^{Calculated}$ and the orange boxes highlight the low HCl concentration experiments.

Comparison of Experimental Data to Previous Experimental Data

Hemley et al. (1992) and Hemley and Hunt (1992) performed the only previous experiments on zinc and lead concentrations in synthetic hydrothermal fluids by using chloride solutions from 300 to 700°C and from 50 to 200 MPa. They used the potassium feldspar-muscovite-quartz mineral assemblage to buffer the HCl concentration of the fluid at each temperature; this limited their concentration data to one HCl condition at each temperature. Hemley et al. (1992) used two different experimental methods. The first method used rocking extraction vessels (i.e. rocking autoclaves) with a platinum delivery tube to obtain 0.5 mL of sample while the experiment was running. This sample was treated with 6 M HCl to remove H_2S

and evaporated to near dryness with perchloric acid to solubilize the metal before being diluted with nitric acid to analyze the metal concentrations with ICP. The second experimental method used cold-seal vessels, which was similar to this study, but after quenching these samples were diluted in nitric acid before being analyzing for metal concentrations using the ICP and AA. Zinc concentrations were detectable whereas lead was generally below detection limits for this method. The lead and zinc solubilities from Hemley et al. (1992) at 300°C were $5.1(\pm0.7)x10^{1}$ µg/g and $3.6(\pm0.1)10^{1}$ µg/g, respectively, at a HCl concentration of $7.28x10^{2}$ µg/g. For 500°C and a HCl concentration of $3.61x10^{3}$ µg/g, lead and zinc concentrations were $3.1(\pm0.5)x10^{3}$ µg/g and $2.7(\pm0.3)x10^{3}$ µg/g, respectively. The concentrations from this study are broadly consistent with those from Hemley et al. (1992), but there are some distinct differences. Hemley et al. (1992) found lead was more soluble that zinc in the hydrothermal fluid and had higher metal concentrations at lower HCl values relative to this study (Figures 10 and 11). The data for lead was only obtained through the extraction vessels method; lead was undetectable using the cold-seal vessels, suggesting that the high lead concentrations of Hemley et al. (1992) may be due to differences in experimental techniques.

Comparison of Experimental Data to Natural Fluid Inclusion Data

Lead and zinc concentration from natural fluid inclusions are extremely variable, even within a single deposit. This is normal since each deposit has various factors that influence deposition, such as source of the fluid, different pulses of ore fluid, surrounding country rock, the duration of the event, and the temperature and pressure of formation. Trends and relationships between metal content, host minerals and mineral assemblages can illuminate important variables. Analyses of fluid inclusions contained within sphalerite and quartz from MVT

deposits have estimated values of lead and zinc from 2 to 350 µg/g and 42 to 150 µg/g, respectively, with salinities of 12 to 25 wt.% NaCl and homogenization temperatures from 51 to 226°C (Appold & Wenz, 2011; Pelch et al., 2015, Stoffell et al., 2008). Fluorite-hosted fluid inclusions from similar deposits had maximum concentrations up to 2000 µg/g lead and 4000 µg/g zinc (Pelch et al., 2015).

The lead and zinc data from this study are generally consistent with the MVT fluid inclusions data with zinc concentrations higher than lead concentrations at lower temperatures. The lead concentrations from the quartz, sphalerite, and fluorite fluid inclusions from MVT deposits are the exception. Most fluid inclusions rarely exceed 100 µg/g lead and were generally consistent with this study. Fluorite-hosted fluid inclusions yielded high lead and zinc that may represent dissolved species in the inclusion fluid (Pelch et al., 2015), as there were only five fluid inclusions above 200 µg/g throughout all of the MVT fluid inclusion studies.

Quartz and sphalerite fluid inclusions from the porphyry-related base metal mineralization for the Morococha District have lead and zinc concentrations of 130 µg/g and 300 µg/g, respectively, with a low salinity of 4.5 wt.% NaCl at 340 to 380°C (Catchpole et al., 2011). A study of quartz fluid inclusions from a porphyry Cu-Au deposit of Bajo de la Alumbrera by Ulrich et al. (2001) examined several different fluid inclusion assemblages throughout the deposit. Their data illustrate zinc and lead concentrations in hydrothermal fluids of 40 to 60 wt.% $NaCl_{eq.}$ are on the order of 8000 and 2200 µg/g in the 500 to 700°C potassic alteration zone, respectively. Zinc and lead concentrations drop to 1500 µg/g and 400 µg/g in lower salinity fluids of 1.4 to 17 wt.% $NaCl_{eq.}$ at 250 to 400°C. A study of the porphyry Cu–Mo deposit at Butte by Rusk et al. (2004) also observed high lead and zinc concentrations of 1008 µg/g and 6060 µg/g, respectively, in a high temperature, saline fluid of 450 to 650°C and 38 wt.% $NaCl_{eq.}$

in the unaltered host-rock zone. As the salinity of the mineralizing fluid dropped in sericitic alteration zone, the lead and zinc concentrations decreased to 60 µg/g and 450 µg/g, respectively, at 3.7 wt.% $NaCl_{eq.}$ from 370 to 450°C. The data that we see in natural deposits are broadly consistent with this study's experimental data. The solubility of both metals drop as HCl concentration and salinity decrease in the system. Temperature is more influential on the solubility of lead, whereas zinc concentrations are less altered by changes in temperature.

Therefore, data from the experiments of this study and fluid inclusions from MVT and porphyry systems suggest that lead and zinc concentrations in a hydrothermal fluid are related directly to salinity, temperature, and HCl concentration. A hydrothermal fluid flowing outward from a melt will precipitate galena and sphalerite in response to a decrease in temperature, salinity and/or HCl concentration, while inducing mineral alteration. Further, the zinc and lead concentrations determined in this study, the first over a range of HCl concentrations, are broadly consistent with data from both porphyry and MVT systems and strongly suggest that HCl and total salinity exert a larger control over metal solubility (and also precipitation) than temperature.

Geological Implications

Mississippi Valley-type Deposits

The physiochemical conditions during transportation and mineralization of MVT deposits have been debated for years. The most cited precipitation mechanism suggests the base metals were transported as chloride complexes in a fluid containing negligible amounts of reduced sulfur. This means reduced sulfur must be added to the fluid by mixing with a pre-existing fluid containing H_2S at the site of deposition or by the reduction of oxidized sulfur (Anderson, 1983;

Sverjensky, 1986). Fluid inclusion studies of the Viburnum Trend, Illinois-Kentucky District, Tri-State, and Northern Arkansas Districts partially support this hypothesis (Appold & Wenz 2011; Pelch et al. 2015; Stoffell et al. 2008). The authors suggest that a fluid, with an assumed moderately acidic pH of 3.5 to 4.5 (Hanor, 1994; 1996), cannot simultaneously carry an anomalously metal-rich fluid along with enough reduced sulfur for precipitation caused by fluid neutralization. Appold and Wenz (2011) determined a mineralizing fluid carrying 1500 µg/g of lead (maximum concentration in this study) would not be able to coexist with the high sulfide concentrations need for precipitation. They suggested that lead was deposited by mixing of metal-rich and sulfur-rich fluids over a timeframe of 10 million years.

The reduced-sulfur model is different from the Appold and Wenz (2011) model in that it proposes the base metals were transported in the fluid together with reduced sulfur and that mineral precipitation occurred as a result of fluid neutralization (change in pH) dilution and/or a decrease in temperature of the fluid (Sverjensky, 1986). Field studies suggest the pH (HCl concentration) of the neutralized ore fluid at the site of deposition is often between 2 and 6 based on the presence of select minerals (i.e. potassium feldspar and dolomite saturation) or dissolved CO_2 (Hanor, 1994, 1996; Plumlee et al., 1991). This large pH range is likely not representative of the hydrothermal fluid that transported lead and zinc to the ore zone, but, rather, the pH during deposition. A study fluid inclusions hosted in sphalerite of the Illinois-Kentucky district estimated a much lower pH of between 0 and 1.4 (Kenderes and Appold, 2017). This study is significant because it suggests that the hydrothermal fluids in MVT deposits may be able to transport higher concentrations of metals and H_2S than was proposed by previous studies which inferred pH values of 2 to 6. The higher metal concentrations and readily avaiable reduced sulfur

would make HCl neutralization the primary precipitation mechanism and greatly reduce the time required for mineralization to 10^4 to 10^5 years.

The data from this study show conclusively that an acidic fluid is capable of dissolving and transporting high concentrations of lead and zinc that can produce a substantial deposit through fluid neutralization (Figure 13). In a MVT style deposit in the southeast Missouri district, a metal-rich, mineralizing fluid moves from the Lamotte sandstone aquifer due to a basement high and encounters the Bonneterre dolostone/limestone. The acidic fluid was neutralized once it interacted with the Bonneterre, decreasing the fluid's HCl and metal concentrations, and inducing precipitation of galena and sphalerite. In the Viburnum Trend, this relationship is observed often as the metal ore resides at or near the contact of the Lamotte sandstone and the Bonneterre dolomite near Precambrian basement highs where the fluid was forced upward into the carbonate (Figure 13). Many MVT deposits are similarly stratabound in limestone or dolostone which has undergone wall rock alteration of either dissolution and hydrothermal brecciation (Anderson, 1975; Appold & Wenz, 2011; Cavender et al., 2016; Corbella et al., 2004; Stoffell et al., 2008; Sverjensky, 1986; Pelch et al., 2015). This carbonization (dolomite or calcite alteration) of the host rock is a result of carbonate minerals becoming unstable in the presents of an acidic fluid (Leach et al., 2010). This evidence of fluid neutralization indicates it plays a substantial role in the precipitation of metals in select MVT deposits.

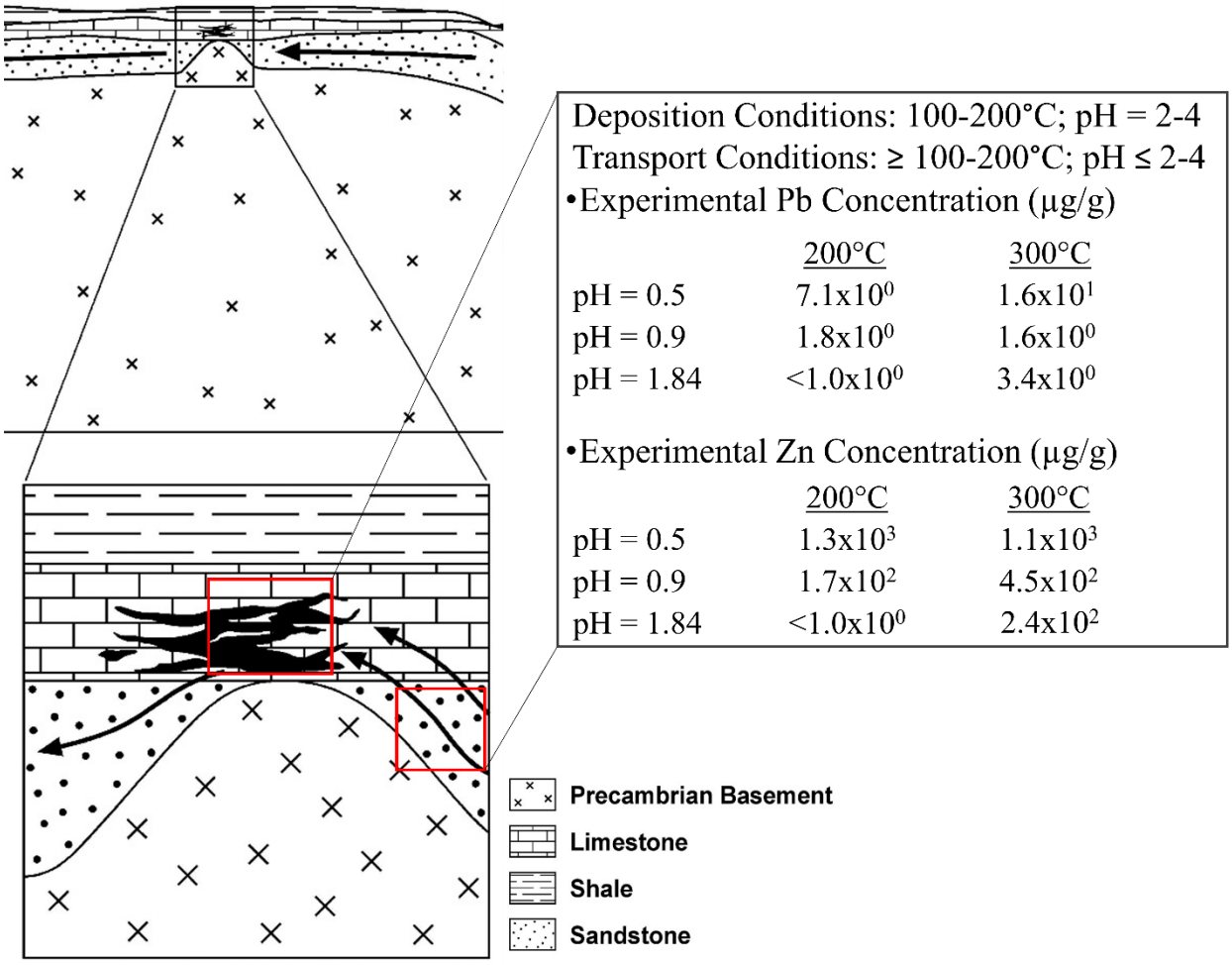

Figure 13: Stratigraphic units in a MVT deposit similar to the Viburnum Trend. Precipitation of the sulfide typically occurs in the carbonate facies. The red boxes highlight the fluid pre-deposition and during deposition. The fluid transporting the metals have a low pH, but once the fluid is neutralized by the carbonate, the increase in pH caused the metal solubility to drop resulting in precipitation.

Porphyry Deposits

Porphyry copper deposits display general trends in metal zoning and alteration assemblages that reveal information about the genesis of the deposit. A magmatic volatile phase exsolved directly from the melt at around 700 to 900°C (Holland, 1972; Sillitoe, 2010) with elements that are incompatible in the crystallizing minerals and travel into the surrounding country rock. As the fluid rises, it experiences a decrease in pressure and temperature while also exchanging elements with the surrounding rock units. These changes induce the precipitation of metal-bearing minerals from the fluid. Ore grade mineralization is favored by a large change in multiple variables over a relatively short distance and/or time interval (Hemley & Hunt, 1992).

Mineral zonation is influenced by changes in pressure and temperature, but is most impacted by fluid-mineral elemental exchange. Hydrothermal alteration involves the replacement of primary minerals as a result elemental exchange with the mineralizing fluid. Progressive changes of the host rock undergoing mineralization can result in a continuously changing mineralizing fluid. Alteration assemblages in magmatic-hydrothermal settings led to a series of commonly recognized alteration zones extending out from the causative igneous intrusion: potassic, sericitic, and propylitic (Figure 14), all with distinct mineral assemblages.

A theoretical calculation was used to determine the maximum HCl concentrations within the potassic alteration zone and at the boundaries of the potassic-sericitic (Frank et al., 1998) and sericitic-propylitic (Hemley and Jones, 1964; Johns et al, 2010), alteration assemblages to illuminate variations in the fluid's composition (Landtwing et al., 2010; Nash, 1976; Seedorff & Einaudi, 2004; Vanko et al., 2001) as it passed through various alteration zones (e.g., Sillitoe, 2010). The physical and chemical properties of the fluids within select alteration assemblages were modeled at each location (Table 5). The composition of the magmatic volatile phase that

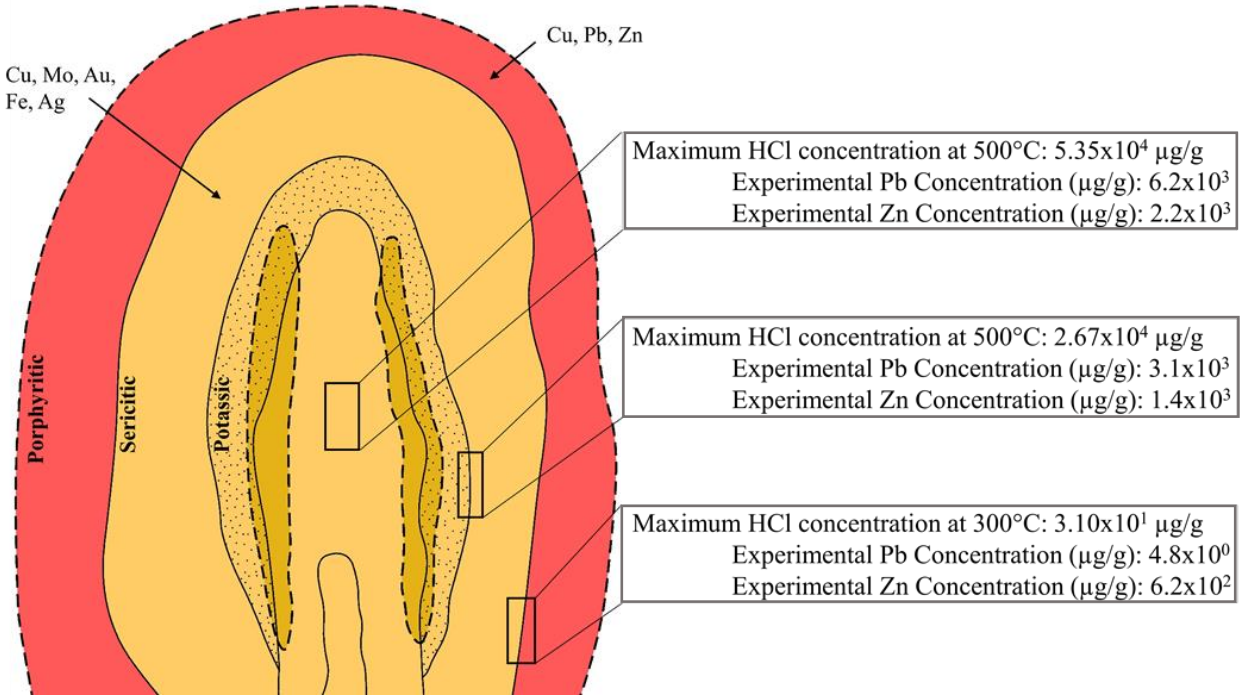

Figure 14: An idealized magmatic-hydrothermal system and alteration assemblages. The estimated HCl concentrations at the boundaries between the alteration zones were calculated from alteration equilibria. The conditions of the fluids are listed in Table 5. The solubility of lead and zinc in the fluid decreases with decreasing temperature and HCl concentrations,

exsolved from the melt was controlled by the elements within the melt and can have high HCl (up to 5 wt.%) and metal concentrations (Holland, 1972; Candela, 1990; Frank et al., 2003).

The potassic alteration zone overlaps the intrusion, represents the highest temperature alteration zone (400 to 800°C), and is only able to slightly buffer the HCl concentration of the fluid. This zone often has highly acidic fluids and can be modeled with the 500°C experimental concentrations of 5.35 x10^4 µg/g HCl. The data from this study suggest that significant lead and zinc can be transported by the fluid in this zone and that galena and sphalerite formation is unlikely. The boundary between the potassic and sericitic alteration (500°C) is marked by a transition from a potassium feldspar, quartz and biotite assemblage to a sericite (muscovite) and quartz assemblage. The production of muscovite at the expense of K-feldspar requires substantial

Table 5: Theoretical conditions of a mineralizing fluid in different alterations zone within a porphyry deposit.

Alteration	Temp.[1] (°C)	Mineral Boundary[2]	ΣCl (wt.% NaCl)[3]	NaCl/KCl (from Kspar-Alb boundary)[4]	Max Salinity (wt.% NaCl)[6]	Max KCl wt.%[6]	KCl/HCl[5]	Max HCl (µg/g)[6]	Max NaCl/HCl [6]	HCl Concentration (µg/g)[6]
Potassic	500	Kspar-Alb	not buffered by surrounding rocks							
Sericitic	500	Musc-Qtz	45	5:1	38	7.5	3.0	2.7	14	$2.7x10^{4}$
Propylitic	300	Pyrop-Alb	15	15:1	14	0.94	300	$3.1x10^{-3}$	4500	31

Kspar= Potassium feldspar, Alb= Albite, Musc= Muscovite, Qtz= Quartz, Pyrop= Pyrophyllite

[1] Johns et al. (2010)

[2] Hemley & Jones (1964); Johns et al. (2010)

[3] Landtwing et al. (2010); Nash (1976); Seedorff & Einaudi (2004); Vanko et al. (2001)

[4] Frank et al. (2018)

[5] Frank et al. (1998); Hemley & Jones (1964)

[6] Calculated value

HCl and the HCl concentration of the fluid drops accordingly to approximately $2.67x10^4$ µg/g. A decrease in HCl results in a decrease of lead and zinc in the fluid and the possible precipitation of minor amounts of galena and sphalerite.

The boundary from sericitic to propylitic alteration (300°C) is indicated by the change to an albite, pyrophyllite, epidote and chlorite assemblage (John et al., 2010). The calculated HCl concentration of $3.10x10^1$ µg/g in the fluid is markedly less than a fluid would have in the potassic and sericitic alteration zones. Accordingly, only tens to hundreds of µg/g of lead and zinc can be transported by the fluid in this zone and, thus, substantial galena and sphalerite precipitation typically occurs.

For the model HCl concentrations, the linear regression from the experimental data were used to calculate the metal concentrations at the alteration boundaries (Figure 14). The HCl concentration of the hydrothermal fluid from the melt decreased through successive mineral alteration reactions that are zoned outward from the core. The solubility of metals in the fluid that are affected by HCl also drop at the transitions between alteration assemblages (Figures 14 and 15). The impact of these rock buffering reactions caused zinc concentrations to decrease by a factor of two between each alteration zone. Lead behaves in a similar manner, expect for the amplified effect of the change in temperature as the fluid moves into the propylitic alteration zone (Figure 14 and 15). This decrease in temperature caused the lead solubility to decrease by a factor of 650. Zinc does not react in the same way as lead with respect to temperature, but the solubility of both metals are controlled by HCl concentrations.

The lead-zinc zone at Bingham is one of the classic examples of base metal zoning in ore deposits. The Bingham Canyon porphyry located in Utah and has geographically well-zoned, metal mineralization (James et al., 1969; Porter et al., 2012). The deposit is comprised of a

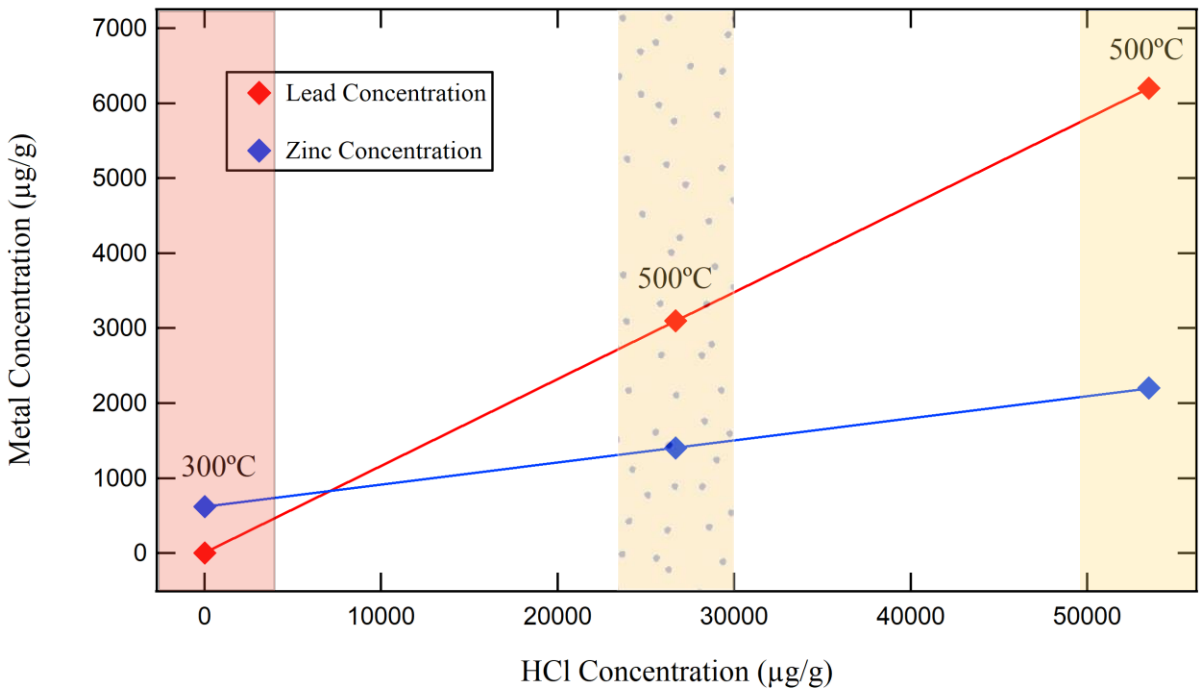

Figure 15: Metal concentrations over a range of HCl concentrations typical of alteration assemblages. Each point is labelled with the corresponding temperature of the alteration assemblage. The colors correspond with the alteration assemblage from Figure 14.

barren core surrounded outwards and upwards by alteration assemblages (Sillitoe 2010). On the periphery of the main copper mineralization, lead-zinc veins and carbonate replacement deposits are located with the most distal lead occurring in unaltered limestone (Jones et al., 1992). The potassic zone remained barren where temperatures and pH were too high to permit significant mineralization. As the fluid moved outward, the temperature and HCl decreased until the solubility was reduced enough for precipitation of galena and sphalerite to occur. The carbonate host rock promoted mineralization as the acidic ore fluid was neutralized in the periphery of the deposit (Hemley & Hunt, 1992).

CHAPTER V
CONCLUSIONS

This study determined the solubility of lead and zinc in synthetic hydrothermal fluids as a function of HCl at 200, 300, and 500°C and are representative of porphyry and MVT style deposits. The synthetic hydrothermal fluid was set to 15 wt.% $NaCl_{eq.}$ and HCl was varied from $2.75x10^2$ to $5.35x10^4$ µg/g to assess its control on metal solubility. Controlling the influential parameters in these ore forming systems, such as composition of the fluid and temperature, allowed us to determine their influence on the metals during ore genesis. Galena and sphalerite, along with the varying NaCl-HCl aqueous fluid, were equilibrated at run conditions in Pt capsules. The post-experiment fluids were captured and analyzed to determine the concentrations of lead and zinc in the fluid at galena- and sphalerite-saturated conditions.

Lead is transported in the hydrothermal fluid as $PbCl_2$ and concentrations were found to range from 1.8±0.2 to $7.9(\pm0.2)x10^3$ µg/g at 200°C ($2.34x10^3$ µg/g of HCl) and 500°C ($5.35x10^4$ µg/g of HCl), respectively. Zinc is transported as $ZnCl_2$ and zinc concentrations followed a similar trend at the same conditions, increasing from $1.7(\pm0.2)x10^2$ to $2.6(\pm0.3)x10^3$ µg/g. Lead and zinc concentrations in the fluid were found to increase directly with HCl concentration. Therefore, decreasing temperature and HCl (increasing pH) are efficient at inducing the precipitation of galena and sphalerite in MVT and porphyry systems. Temperature changes induced greater changes in the lead concentrations of the fluid than zinc. This demonstrates that

the variable Pb:Zn ratios observed in some ore-bearing systems may be partially attributed to differences in the rate of change of temperature, acidity, and/or reduced sulfur.

The data from this study was evaluated relative to the two deposit types that produce the most lead and zinc. Porphyry style deposits contain significant base metal mineralization of lead and zinc in distal veins and orebodies. Mineralization in these systems is often attributed to decreases in temperature and/or an increase in pH. Many of the lead- and zinc-rich systems are associated with carbonate host rock. Porphyry systems which intrude carbonate minerals are referred to as skarns since the mineral zonation is slightly different than a typical porphyry deposits. The carbonate host rocks efficiently neutralize the fluid's HCl content, decreasing the fluid's ability to transport $PbCl_2$ and $ZnCl_2$, and thus induce the precipitation of lead and zinc as galena and sphalerite within a smaller volume of rock than in systems where silicate minerals dominate.

MVT deposits do not see significant deviations in temperature from the source zone to the area of deposition so the neutralization of HCl or the addition of reduced sulfur are the most likely precipitation mechanisms. Lead- and zinc-bearing MVT deposits were previously believed to only have a moderately acidic pH and were not capable of transporting enough metals and reduced sulfur together for the observed mineralization. Thus, the addition of reduced sulfur was thought to be the dominant reason for galena and sphalerite precipitation. However, recent studies of natural systems have demonstrated that, at least for a number of deposits, the mineralizing fluid had a much lower pH (higher HCl concentration) than previously documented. The data from this study shows conclusively that an acidic fluid similar to that recently documented is capable of containing high concentrations of lead, zinc, and reduced sulfur and can produce a substantial deposit through fluid neutralization. Wall rock alteration in these

systems and the abundance of lead and zinc are the contact between sandstone and carbonate units is evidence that neutralization of the fluid's HCl concentration plays a dominant role in the precipitation of metals in MVT deposits.

Therefore, the HCl concentration in both synthetic and natural hydrothermal fluids is well defined in controlling the transportation of lead and zinc and the precipitation of galena and sphalerite in all ore systems. Data from this study and the analyses of natural deposits suggest that the exploration for galena and sphalerite deposits should focus on lower temperature zones and on rock units (or contacts) that have the capacity to neutralize the HCl within the hydrothermal fluid, as this will promote mineralization.

REFERENCES

Allan, M. M., Morrison, G. W., & Yardley, B. W. (2011). Physicochemical evolution of a porphyry-breccia system: a laser ablation ICP-MS study of fluid inclusions in the Mount Leyshon Au Deposit, Queensland, Australia. *Economic Geology, 106*(3), pp. 413-436.

Anderko, A., & Pitzer, K. S. (1993). Phase equilibria and volumetric properties of the systems KCl-H2O and NaCl-KCl-H2O above 573 K: Equation of state representation. *Geochimica et Cosmochimica Acta, 57*(20), pp. 4885-4897.

Anderson, G. M. (1975). Precipitation of Mississippi Valley-type ores. *Economic Geology, 70*(5), pp. 937-942.

Anderson, G. M. (1983). Some geochemical aspects of sulfide precipitation in carbonate rocks. *International Conference on Mississippi Valley Type Lead-Zinc Deposits*, pp. 61-76.

Anderson, G. M., & Macqueen, R. W. (1982). Ore deposit models-6. Mississippi Valley-type lead-zinc deposits. *Geoscience Canada, 9*(2), pp. 108-117.

Appold, M. S., & Wenz, Z. J. (2011). Composition of ore fluid inclusions from the viburnum trend, southeast Missouri district, United States: Implications for transport and precipitation mechanisms. *Economic Geology, 106*(1), pp. 55-78.

Barton, P. B., & Toulmin, P. (1966). Phase relations involving sphalerite in the Fe-Zn-S system. *Economic Geology, 61*(5), pp. 815-849.

Bodnar, R. J., Burnham, C. W., & Sterner, S. M. (1985). Synthetic fluid inclusions in natural quartz. III. Determination of phase equilibrium properties in the system H2O-NaCl to 1000°C and 1500 bars. *Geochimica et Cosmochimica Acta, 49*(9), pp. 1861-1873.

Bradley, D. C., & Leach, D. L. (2003). Tectonic controls of Mississippi valley-type lead-zinc mineralization in orogenic forelands. *Mineralium Deposita, 38*(6), pp. 652-667.

Burnham, C. W. (1979). *Geochemistry of Hydrothermal Ore Deposits*. New York, NY: John Wiley & Sons.

Candela, P. A., & Holland, H. D. (1984). The partitioning of copper and molybdenum between silicate melts and aqueous fluids. *Geochimica et Cosmochimica Acta, 48*(2), pp. 373-380.

Cavender, B. D., Shelton, K. L., & Schiffbauer, J. D. (2016). An atypical orebody in the Brushy Creek Mine, Viburnum Trend, MVT district, Missouri: Early Cu-(Ni-Co)-Zn-rich ores at the Lamotte sandstone/Bonneterre dolomite contact. *Economic Geology, 111*(1), pp. 259-269.

Catchpole, H., Kouzmanov, K., Fontbote, L., Guillong, M., & Heinrich, C. A. (2011). Fluid evolution in zoned cordilleran polymetallic veins; insights from microthermometry and LA-ICP-MS of fluid inclusions. *Chemical Geology, 281*(3-4), pp. 293-304.

Cook, N. J., Ciobanu, C. L., Pring, A., Skinner, W., Shimizu, M., Danyushevsky, L., Saint-Eidukat, B. & Melcher, F. (2009). Trace and minor elements in sphalerite: A LA-ICPMS study. *Geochimica et Cosmochimica Acta, 73*(16), pp. 4761-4791.

Corbella, M., Ayora, C., & Cardellach, E. (2004). Hydrothermal mixing, carbonate dissolution and sulfide precipitation in Mississippi Valley-type deposits. *Mineralium Deposita, 39*(3), pp. 344-357.

Frank, M. R., Candela, P. A., & Piccoli, P. M. (1998). K-feldspar-muscovite-andalusite-quartz-brine phase equilibria: An experimental study at 25 to 60 MPa and 400 to 550 C. *Geochimica et Cosmochimica Acta, 62*(23-24), pp. 3717-3727.

Frank, M. R., Candela, P. A., Piccoli, P. M., & Glascock, M. D. (2002). Gold solubility, speciation, and partitioning as a function of HCl in the brine-silicate melt-metallic gold system at 800 degrees C and 100 MPa. *Geochimica et Cosmochimica Acta, 66*(21), pp. 3719-3732.

Frank, M. R., Simon, A. C., Pettke, T., Candela, P. A., & Piccoli, P. M. (2011). Gold and copper partitioning in magmatic-hydrothermal systems at 800 degrees C and 100 MPa. *Geochimica et Cosmochimica Acta, 75*(9), pp. 2470-2482.

Frank, M. R., Fraley, K., Kerwin, S. &Vaccaro, D. (2018). Feldspar-Brine Alteration at High-Temperatures. *Manuscript submitted for publication*.

Garven, G., & Appold, M. S. (1998). Hydrogeologic modeling of the genesis of carbonate-hosted lead-zinc ores. *Hydrogeology Journal, 7*(1), pp. 108-126.

Giordano, T. H., & Barnes, H. L. (1979). Ore solution chemistry VI; PbS solubility in bisulfide solutions to 300 degrees C. *Economic Geology, 74*(7), pp. 1637-1646.

Giordano, T. H., & Barnes, H. L. (1981). Lead transport in Mississippi Valley-type ore solutions. *Economic Geology, 76*(8), pp. 2200-2211.

Hanor, J. S. (1994). Origin of saline fluids in sedimentary basins. *Geological Society, London, Special Publications, 78*(1), pp. 151-174.

Hanor, J. S. (1996). Controls on the solubilization of lead and zinc in basinal brines. *Society of Economic Geologists Special Publication, 4*, pp. 483−500.

Hedenquist, J. W., Arribas, A., & Reynolds, T. J. (1998). Evolution of an intrusion-centered hydrothermal system; Far Southeast-Lepanto porphyry and epithermal Cu-Au deposits, Philippines. *Economic Geology, 93*(4), pp. 373-404.

Heinrich, C. A. (2005). The physical and chemical evolution of low-salinity magmatic fluids at the porphyry to epithermal transition: a thermodynamic study. *Mineralium Deposita, 39*(8), pp. 864-889.

Heinrich, C. A., Gunther, D., Audétat, A., Ulrich, T., & Frischknecht, R. (1999). Metal fractionation between magmatic brine and vapor, determined by microanalysis of fluid inclusions. *Geology, 27*(8), pp. 755-758.

Hemley, J. J. (1953). A study of lead sulfide solubility and its relation to ore deposition. *Economic Geology*, *48*(2), pp. 113-138.

Hemley, J. J., & Jones, W. R. (1964). Chemical aspects of hydrothermal alteration with emphasis on hydrogen metasomatism. Economic *Geology, 59*(4), pp. 538-569.

Hemley, J. J., Cygan, G. L., Fein, J. B., Robinson, G. R., & D'Angelo, W. M. (1992). Hydrothermal ore-forming processes in the light of studies in rock-buffered systems: I. Iron-copper-zinc-lead sulfide solubility relations. *Economic Geology, 87*(1), pp. 1-22.

Hemley, J. J., & Hunt, J. P. (1992). Hydrothermal ore-forming processes in the light of studies in rock-buffered systems: II. Some general geologic applications. *Economic Geology, 87*(1), pp. 23-43.

Holland, H. D. (1972). Granites, Solutions, and Base Metal Deposits. *Economic Geology and the Bulletin of the Society of Economic Geologists, 67*(3), pp. 281-301.

Huehner, S. H., & Sato, M. (1970). The oxygen fugacity-temperature relationships of manganese oxide and nickel oxide buffers. *The American Mineralogist, 55*, pp. 934-952.

İmer, A., Richards, J. P., & Muehlenbachs, K. (2016). Hydrothermal Evolution of the Çöpler Porphyry-Epithermal Au Deposit, Erzincan Province, Central Eastern Turkey. *Economic Geology, 111*(7), pp. 1619-1658.

James, A., Smith, W., Bray, R. E. & John, E. C. (1969). Bingham District- A zoned porphyry ore deposit. *Bulletin- Utah Geological and Mineralogical Survey*, pp. 200-213.

John, D. A., Ayuso, R. A., Barton, M. D., Blakely, R. J., Bodnar, R. J., Dilles, J. H., Gray, F., Graybeal, F. T., Mars, J. C., McPhee, D. K., Seal, R. R., Taylor, R. D. & Vikre, P. G. (2010). Porphyry copper deposit model. *Scientific investigations report*.

Jones, H. D., & Kesler, S. E. (1992). Fluid inclusion gas chemistry in east Tennessee Mississippi Valley-type districts: evidence for immiscibility and implications for depositional mechanisms. *Geochimica et Cosmochimica Acta*, *56*(1), pp. 137-154.

Kenderes, S. M., & Appold, M. S. (2017). Fluorine concentrations of ore fluids in the Illinois-Kentucky district: Evidence from SEM-EDS analysis of fluid inclusion decrepitates. *Geochimica et Cosmochimica Acta, 210*, pp. 132-151.

Kesler, S. E., Gesink, J. A., & Haynes, F. M. (1989). Evolution of mineralizing brines in the east Tennessee Mississippi Valley-type ore field. *Geology, 17*(5), pp. 466-469.

Landtwing, M. R., Furrer, C., Redmond, P. B., Pettke, T., Guillong, M., & Heinrich, C. A. (2010). The Bingham Canyon porphyry Cu-Mo-Au deposit. III. Zoned copper-gold ore deposition by magmatic vapor expansion. *Economic Geology, 105*(1), pp. 91-118.

Lawley, C. M., Richards, J. P., Anderson, R. G., Creaser, R. A., & Heaman, L. M. (2010). Geochronology and geochemistry of the MAX porphyry Mo deposit and its relationship to Pb-Zn-Ag mineralization, Kootenay Arc, southeastern British Columbia, Canada. *Economic Geology, 105*(6), pp. 1113-1142.

Leach, D. L., Taylor, R. D., & Fey, D. L. (2010). A deposit model for Mississippi valley-type lead-zinc ores. *Mineral Deposit Models for Resource Assessment: U.S. Geological Survey Scientific Investigations Report* (5070-A). Reston, VA. U.S. Geological Survey.

Lowell, J. D., & Guilbert, J. M. (1970). Lateral and vertical alteration-mineralization zoning in porphyry ore deposits. *Economic Geology, 65*(4), pp. 373-408.

Meinert, L. D. (1987). Skarn zonation and fluid evolution in the Groundhog mine, Central mining district, New Mexico. *Economic Geology, 82*(3), pp. 523-545.

Meinert, L. D. (1992). Skarns and skarn deposits. *Geoscience Canada, 19*(4), pp. 145-162.

Meinert, L. D., Hedenquist, J. W., Satoh, H., & Matsuhisa, Y. (2003). Formation of anhydrous and hydrous skarn in Cu-Au ore deposits by magmatic fluids. *Economic Geology, 98*(1), pp. 147-156.

Nash, J. T. (1976). Fluid-inclusion petrology- Data from porphyry copper deposits and applications to exploration. *Geology and resources of copper deposits: Geological Survey Professional Paper* (907-D). Washington, D.C. U.S. Government Printing Office.

Pelch, M. A., Appold, M. S., Emsbo, P., & Bodnar, R. J. (2015). Constraints from fluid inclusion compositions on the origin of Mississippi Valley-type mineralization in the Illinois-Kentucky District. *Economic Geology, 110*(3), pp. 787-808.

Porter, J. P., Schroeder, K., & Austin, G. (2012). Geology of Bingham Canyon porphyry Cu-Mo-Au deposit, Utah. *Society of Economic Geologist, Special Publication, 16*, pp. 127-146.

Pitzer, K. S., Peiper, J. C., & Busey, R. H. (1984). Thermodynamic properties of aqueous sodium chloride solutions. *Journal of Physical and Chemical Reference Data, 13*(1), pp. 1-102.

Plumlee, G. S., Leach, D. L., Hofstra, A. H., Landis, G. P., Rowan, E. L., & Viets, J. G. (1994). Chemical reaction path modeling of ore deposition in Mississippi Valley-type Pb-Zn deposits of the Ozark region, US Midcontinent. *Economic Geology, 89*(6), pp. 1361-1383.

Pokrovski, G. S., Roux, J., & Harrichoury, J. C. (2005). Fluid density control on vapor-liquid partitioning of metals in hydrothermal systems. *Geology, 33*(8), pp. 657-660.

Pokrovski, G. S., Borisova, A. Y., & Bychkov A. Y. (2013) The effect of sulfur on vapor-liquid fractionation of metals in hydrothermal systems. *Reviews in Mineralogy & Geochemistry, 76*, pp. 165-218.

Robb, L. (2005). *Introduction to Ore-forming Processes*. Hoboken, NJ: Blackwell Publishing Company.

Rusk, B. G., Reed, M. H., Dilles, J. H., Klemm, L. M., & Heinrich, C. A. (2004). Compositions of magmatic hydrothermal fluids determined by LA-ICP-MS of fluid inclusions from the porphyry copper–molybdenum deposit at Butte, MT. *Chemical Geology, 210*(1-4), pp. 173-199.

Seedorff, E., & Einaudi, M. T. (2004). Henderson porphyry molybdenum system, Colorado: I. Sequence and abundance of hydrothermal mineral assemblages, flow paths of evolving fluids, and evolutionary style. *Economic Geology, 99*(1), pp. 3-37.

Sillitoe, R. H. (1997). Characteristics and controls of the largest porphyry copper-gold and epithermal gold deposits in the circum-Pacific region. *Australian Journal of Earth Sciences, 44*(3), pp. 373-388.

Sillitoe, R. H. (2010). Porphyry copper deposit. *Economic Geology, 105*, pp. 3-41.

Stoffell, B., Appold, M. S., Wilkinson, J. J., McClean, N. A., & Jeffries, T. E. (2008). Geochemistry and evolution of Mississippi Valley-type mineralizing brines from the Tri-State and Northern Arkansas Districts determined by LA-ICP-MS microanalysis of fluid inclusions. *Economic Geology, 103*(7), pp. 1411-1435.

Sverjensky, D. A. (1981). The origin of a Mississippi valley-type deposit in the viburnum trend, southeast Missouri. *Economic Geology, 76*(7), pp. 1848-1872.

Sverjensky, D. A. (1986). Genesis of Mississippi valley-type lead-zinc deposits. *Annual Review of Earth and Planetary Sciences, 14*(1), pp. 177-199.

Titley, S. R. (1996). Characteristics of high temperature, carbonate-hosted replacement ores and some comparisons with Mississippi Valley-type ores. *Society of Economic Geologist, Special Publication, 4*, pp. 244-254.

Ulrich, T., Günther, D., & Heinrich, C. A. (2002). The evolution of a porphyry Cu-Au deposit, based on LA-ICP-MS analysis of fluid inclusions: Bajo de la Alumbrera, Argentina. *Economic Geology, 97*(8), pp. 1889-1920.

Vanko, D. A., Bonnin-Mosbah, M., Philippot, P., Roedder, E., & Sutton, S. R. (2001). Fluid inclusions in quartz from oceanic hydrothermal specimens and the Bingham, Utah porphyry-Cu deposit: a study with PIXE and SXRF. *Chemical Geology*, *173*(1-3), pp. 227-238.

Williams-Jones, A. E., & Heinrich, C. A. (2005). 100th Anniversary special paper: Vapor transport of metals and the formation of magmatic-hydrothermal ore deposits. *Economic Geology*, *100*(7), pp. 1287-1312.

APPENDIX I

RAW SEM DATA

Pre-Experiment							
	Galena			Sphalerite			
Analysis	**S wt%**	**Pb wt%**	**Total**	**S wt%**	**Zn wt%**	**Fe wt%**	**Total**
1	13.66	86.34	100.00	33.49	66.51	0.00	100.00
2	14.02	85.98	100.00	36.35	63.18	0.47	100.00
3	13.52	86.48	100.00	36.71	62.97	0.32	100.00
4	14.47	85.53	100.00	37.41	62.59	0.00	100.00
5	14.30	85.70	100.00	35.81	63.67	0.52	100.00
6	14.24	85.76	100.00	35.78	64.22	0.00	100.00
7	14.40	85.60	100.00	33.86	66.14	0.00	100.00
8	14.42	85.58	100.00	35.14	64.86	0.00	100.00
9	14.27	85.73	100.00	36.58	63.42	0.00	100.00
10	13.30	86.70	100.00	35.99	64.01	0.00	100.00
AVE	14.06	85.94	100.00	35.712	64.157	0.13	100.00
STD	0.40	0.40		1.18	1.25	0.21	

E1C2							
	Galena			Sphalerite			
Analysis	**S wt%**	**Pb wt%**	**Total**	**S wt%**	**Zn wt%**	**Fe wt%**	**Total**
1	10.70	89.30	100.00	32.19	67.81	0.00	100.00
2	10.52	89.48	100.00	29.68	70.32	0.00	100.00
3	10.23	89.77	100.00	28.3	71.70	0.00	100.00
4	8.82	91.18	100.00	32.25	67.75	0.00	100.00
5	9.36	90.64	100.00	29.32	70.68	0.00	100.00
AVE	9.93	90.07	100.00	29.83	70.17	0.00	100.00
STD	0.72	0.72		1.86	1.86	0.00	

E2C3							
	Galena			Sphalerite			
Analysis	**S wt%**	**Pb wt%**	**Total**	**S wt%**	**Zn wt%**	**Fe wt%**	**Total**
1	10.02	89.98	100.00	25.66	74.34	0.00	100.00
2	9.73	90.27	100.00	31.62	68.38	0.00	100.00
3	10.53	89.47	100.00	28.24	71.76	0.00	100.00
4	9.65	90.35	100.00	31.62	68.38	0.00	100.00
5	11.71	88.29	100.00	30.45	69.55	0.00	100.00
AVE	10.33	89.67	100.00	29.52	70.48	0.00	100.00
STD	0.76	0.76		2.29	2.29	0.00	

E2C4							
	Galena			Sphalerite			
Analysis	**S wt%**	**Pb wt%**	**Total**	**S wt%**	**Zn wt%**	**Fe wt%**	**Total**

1	10.02	89.98	100.00	30.31	69.69	0.00	100.00
2	9.73	90.27	100.00	29.29	70.71	0.00	100.00
3	10.53	89.47	100.00	30.99	69.01	0.00	100.00
4	9.65	90.35	100.00	32.14	67.86	0.00	100.00
5	11.71	88.29	100.00	32.6	67.4	0.00	100.00
AVE	10.33	89.67	100.00	31.07	68.93	0.00	100.00
STD	0.76	0.76		1.20	1.20	0.00	

E3C6							
	Galena			**Sphalerite**			
Analysis	**S wt%**	**Pb wt%**	**Total**	**S wt%**	**Zn wt%**	**Fe wt%**	**Total**
1	10.48	89.52	100.00	30.25	69.75	0.00	100.00
2	9.45	90.55	100.00	30.18	69.82	0.00	100.00
3	8.80	91.20	100.00	29.53	70.47	0.00	100.00
4	10.22	89.78	100.00	31.06	68.94	0.00	100.00
5	8.41	91.59	100.00	28.82	71.18	0.00	100.00
AVE	9.47	90.53	100.00	27.96	72.04	0.00	100.00
STD	0.79	0.79		4.54	4.54	0.00	

E4C8							
	Galena			**Sphalerite**			
Analysis	**S wt%**	**Pb wt%**	**Total**	**S wt%**	**Zn wt%**	**Fe wt%**	**Total**
1	10.76	89.24	100.00	28.12	71.88	0.00	100.00
2	10.03	89.97	100.00	29.56	70.44	0.00	100.00
3	10.32	89.68	100.00	31.74	68.26	0.00	100.00
4	10.28	89.72	100.00	33.04	66.96	0.00	100.00
6	10.06	89.94	100.00	31.25	68.75	0.00	100.00
7	10.29	89.71	100.00	30.74	69.26	0.00	100.00
AVE	10.29	89.71	100.00	30.74	69.26	0.00	100.00
STD	0.24	0.24		1.57	1.57		

E5C10							
	Galena			**Sphalerite**			
Analysis	**S wt%**	**Pb wt%**	**Total**	**S wt%**	**Zn wt%**	**Fe wt%**	**Total**
1	11.77	88.23	100.00	31.24	68.76	0.00	100.00
2	10.14	89.86	100.00	30.81	69.19	0.00	100.00
3	9.16	90.84	100.00	31.95	68.05	0.00	100.00
4	11.83	88.17	100.00	27.75	72.25	0.00	100.00
5	11.05	88.95	100.00	29.5	70.5	0.00	100.00
6	10.79	89.21	100.00	30.25	69.75	0.00	100.00
AVE	10.79	89.21	100.00	30.25	69.75	0.00	100.00

STD	0.93	0.93		1.35	1.35	0.00	

E5C11							
	Galena			**Sphalerite**			
Analysis	**S wt%**	**Pb wt%**	**Total**	**S wt%**	**Zn wt%**	**Fe wt%**	**Total**
1	12.71	87.29	100.00	28.42	71.58	0.00	100.00
2	13.11	86.89	100.00	32.36	67.64	0.00	100.00
3	12.60	87.40	100.00	32.14	67.86	0.00	100.00
4	12.84	87.16	100.00	28.87	71.13	0.00	100.00
5	11.86	88.14	100.00	35.17	64.83	0.00	100.00
AVE	12.62	87.38	100.00	31.39	68.61	0.00	100.00
STD	0.42	0.42		2.49	2.49	0.00	

E6C12							
	Galena			**Sphalerite**			
Analysis	**S wt%**	**Pb wt%**	**Total**	**S wt%**	**Zn wt%**	**Fe wt%**	**Total**
1	13.60	86.40	100.00	29.48	70.52	0.00	100.00
2	14.14	85.86	100.00	29.92	70.08	0.00	100.00
3	13.17	86.83	100.00	29.61	70.39	0.00	100.00
4	13.19	86.81	100.00	29.7	70.3	0.00	100.00
5	13.83	86.17	100.00	29.93	70.07	0.00	100.00
6	13.04	86.96	100.00	29.79	70.21	0.00	100.00
7	12.60	87.40	100.00	29.75	70.25	0.00	100.00
8	13.03	86.97	100.00	29.82	70.18	0.00	100.00
9	13.37	86.63	100.00	29.57	70.43	0.00	100.00
10	12.52	87.48	100.00	29.66	70.34	0.00	100.00
AVE	13.25	86.75	100.00	29.72	70.28	0.00	100.00
STD	0.48	0.48		0.14	0.14	0.00	

E7C14							
	Galena			**Sphalerite**			
Analysis	**S wt%**	**Pb wt%**	**Total**	**S wt%**	**Zn wt%**	**Fe wt%**	**Total**
1	13.15	86.85	100.00	29.4	70.1	0.5	100.00
2	13.30	86.70	100.00	29.65	70.35	0.00	100.00
3	13.18	86.82	100.00	31.02	68.98	0.00	100.00
4	13.46	86.54	100.00	29.52	70.48	0.00	100.00
5	12.81	87.19	100.00	30.45	69.55	0.00	100.00
6	13.37	86.63	100.00	30.32	69.68	0.00	100.00
7	13.66	86.34	100.00	29.54	70.46	0.00	100.00
8	14.29	85.71	100.00	29.03	70.97	0.00	100.00
9	12.99	87.01	100.00	29.42	70.58	0.00	100.00

10	13.27	86.73	100.00	29.44	70.56	0.00	100.00
11	12.92	87.08	100.00	29.779	70.171	0.05	100.00
AVE	13.31	86.69	100.00	29.78	70.17	0.05	100.00
STD	0.39	0.39		0.55	0.54	0.14	

E8C16							
	Galena			**Sphalerite**			
Analysis	**S wt%**	**Pb wt%**	**Total**	**S wt%**	**Zn wt%**	**Fe wt%**	**Total**
1	13.55	86.45	100.00	30.9	69.1	0.00	100.00
2	13.80	86.20	100.00	29.73	70.27	0.00	100.00
3	13.62	86.38	100.00	30.51	69.49	0.00	100.00
4	13.75	86.25	100.00	29.92	70.08	0.00	100.00
5	13.03	86.97	100.00	28.48	71.52	0.00	100.00
6	14.75	85.25	100.00	29.25	70.75	0.00	100.00
7	12.97	87.03	100.00	30.27	69.73	0.00	100.00
8	13.65	86.35	100.00	29.09	70.91	0.00	100.00
9	12.84	87.16	100.00	29.1	70.9	0.00	100.00
10	13.68	86.32	100.00	31.39	68.61	0.00	100.00
AVE	13.56	86.44	100.00	29.86	70.14	0.00	100.00
STD	0.52	0.52		0.86	0.86	0.00	

E9C17							
	Galena			**Sphalerite**			
Analysis	**S wt%**	**Pb wt%**	**Total**	**S wt%**	**Zn wt%**	**Fe wt%**	**Total**
1	13.55	86.45	100.00	28.87	70.85	0.28	100.00
2	13.31	86.69	100.00	30.19	69.52	0.29	100.00
3	12.43	87.57	100.00	29.82	70.18	0.00	100.00
4	13.40	86.60	100.00	29.15	70.85	0.00	100.00
5	13.72	86.28	100.00	28.91	71.09	0.00	100.00
6	13.63	86.37	100.00	29.25	70.75	0.00	100.00
7	13.61	86.39	100.00	29.4	70.6	0.00	100.00
8	12.59	87.41	100.00	30.2	69.8	0.00	100.00
9	13.08	86.92	100.00	30.23	69.39	0.38	100.00
10	12.32	87.68	100.00	29.93	69.72	0.35	100.00
AVE	13.16	86.84	100.00	29.60	70.28	0.13	100.00
STD	0.50	0.50		0.51	0.60	0.16	

E10C18							
	Galena			**Sphalerite**			
Analysis	**S wt%**	**Pb wt%**	**Total**	**S wt%**	**Zn wt%**	**Fe wt%**	**Total**
1	13.22	86.78	100.00	29.04	70.96	0.00	100.00

2	12.73	87.27	100.00	28.21	71.79	0.00	100.00
3	12.90	87.11	100.01	29.21	70.79	0.00	100.00
4	13.32	86.68	100.00	29.32	70.68	0.00	100.00
5	13.38	86.62	100.00	30.95	69.05	0.00	100.00
6	14.20	85.80	100.00	30.5	69.5	0.00	100.00
7	12.78	87.22	100.00	30.5	69.19	0.31	100.00
8	14.39	85.61	100.00	30.51	69.49	0.00	100.00
9	13.33	86.67	100.00	31.3	68.23	0.47	100.00
10	13.33	86.67	100.00	29.24	70.76	0.00	100.00
AVE	13.36	86.64	100.00	29.88	70.04	0.08	100.00
STD	0.52	0.52		0.95	1.05	0.16	

E10C20							
	Galena			**Sphalerite**			
Analysis	**S wt%**	**Pb wt%**	**Total**	**S wt%**	**Zn wt%**	**Fe wt%**	**Total**
1	12.53	87.47	100.00	30.26	69.74	0.00	100.00
2	12.34	87.66	100.00	29.15	70.85	0.00	100.00
3	12.46	87.54	100.00	29.86	70.14	0.00	100.00
4	12.46	87.54	100.00	29.97	70.03	0.00	100.00
5	12.83	87.17	100.00	30.75	69.25	0.00	100.00
6	12.34	87.66	100.00	30.95	69.05	0.00	100.00
7	13.52	86.48	100.00	31.84	68.16	0.00	100.00
8	8.71	91.29	100.00	29.56	70.44	0.00	100.00
9	9.85	90.15	100.00	30.18	69.82	0.00	100.00
10	12.34	87.66	100.00	30.57	69.43	0.00	100.00
AVE	11.94	88.06	100.00	30.31	69.69	0.00	100.00
STD	1.39	1.39		0.73	0.73	0.00	

E11C21							
	Galena			**Sphalerite**			
Analysis	**S wt%**	**Pb wt%**	**Total**	**S wt%**	**Zn wt%**	**Fe wt%**	**Total**
1	13.39	86.61	100.00	29.81	70.19	0.00	100.00
2	12.81	87.19	100.00	30.43	69.57	0.00	100.00
3	12.91	87.09	100.00	31.26	68.74	0.00	100.00
4	13.56	86.44	100.00	32.38	67.62	0.00	100.00
5	13.65	86.35	100.00	30.34	69.66	0.00	100.00
6	13.25	86.75	100.00	30.89	69.11	0.00	100.00
8	12.65	87.35	100.00	31.79	68.21	0.00	100.00
9	13.29	86.71	100.00	30.41	69.59	0.00	100.00
10	13.35	86.65	100.00	30.66	69.34	0.00	100.00
AVE	13.21	86.79	100.00	30.89	69.11	0.00	100.00

STD	0.32	0.32		0.76	0.76	0.00	

E11C22							
	Galena			**Sphalerite**			
Analysis	**S wt%**	**Pb wt%**	**Total**	**S wt%**	**Zn wt%**	**Fe wt%**	**Total**
1	13.29	86.71	100.00	29.74	70.26	0.00	100.00
2	12.98	87.02	100.00	31.43	68.57	0.00	100.00
3	13.56	86.44	100.00	30.62	69.38	0.00	100.00
4	13.82	86.18	100.00	29.65	70.35	0.00	100.00
5	14.02	85.98	100.00	30.54	69.46	0.00	100.00
6	12.96	87.04	100.00	29.73	70.27	0.00	100.00
7	13.80	86.20	100.00	30.38	69.62	0.00	100.00
8	13.80	86.20	100.00	31.48	68.52	0.00	100.00
9	14.11	85.89	100.00	30.52	69.48	0.00	100.00
10	14.37	85.63	100.00	30.31	69.69	0.00	100.00
AVE	13.67	86.33	100.00	30.44	69.56	0.00	100.00
STD	0.45	0.45		0.61	0.61	0.00	

E12C23							
	Galena			**Sphalerite**			
Analysis	**S wt%**	**Pb wt%**	**Total**	**S wt%**	**Zn wt%**	**Fe wt%**	**Total**
11	14.00	86.00	100.00	30.08	69.92	0.00	100.00
2	13.70	86.30	100.00	29.7	70.3	0.00	100.00
3	13.62	86.38	100.00	29.9	69.76	0.34	100.00
4	14.00	86.00	100.00	29.18	70.82	0.00	100.00
5	13.30	86.70	100.00	29.36	70.23	0.41	100.00
6	13.19	86.81	100.00	29.17	70.83	0.00	100.00
7	13.51	86.49	100.00	30.26	69.74	0.00	100.00
8	13.20	86.80	100.00	30.75	68.8	0.45	100.00
9	13.09	86.91	100.00	30.39	69.61	0.00	100.00
10	14.01	85.99	100.00	29.29	70.43	0.28	100.00
AVE	13.56	86.44	100.00	29.81	70.04	0.15	100.00
STD	0.34	0.34		0.53	0.58	0.19	

E13C24							
	Galena			**Sphalerite**			
Analysis	**S wt%**	**Pb wt%**	**Total**	**S wt%**	**Zn wt%**	**Fe wt%**	**Total**
1	11.69	88.31	100.00	26.67	72.95	0.38	100.00
2	12.57	87.43	100.00	29.61	70.39	0.00	100.00
3	12.26	87.74	100.00	26.53	73.01	0.46	100.00
4	11.29	88.71	100.00	26.54	73.17	0.29	100.00

5	12.13	87.87	100.00	27.1	72.9	0.00	100.00
6	12.02	87.98	100.00	28.48	71.52	0.00	100.00
7	12.33	87.67	100.00	27.12	72.88	0.00	100.00
8	12.34	87.66	100.00	28.95	70.76	0.29	100.00
9	12.83	87.17	100.00	27.73	72.27	0.00	100.00
10	13.18	86.82	100.00	28.57	71.43	0.00	100.00
AVE	12.26	87.74	100.00	27.73	72.13	0.14	100.00
STD	0.51	0.51		1.05	0.97	0.18	

E13C25							
	Galena			**Sphalerite**			
Analysis	**S wt%**	**Pb wt%**	**Total**	**S wt%**	**Zn wt%**	**Fe wt%**	**Total**
1	12.07	87.94	100.01	28.3	71.7	0.00	100.00
3	11.69	88.31	100.00	28.28	71.72	0.00	100.00
4	12.50	87.50	100.00	28.49	71.51	0.00	100.00
5	12.23	87.77	100.00	28.43	71.57	0.00	100.00
6	12.44	87.56	100.00	28.53	71.47	0.00	100.00
7	12.31	87.69	100.00	28.39	71.34	0.27	100.00
8	13.77	86.23	100.00	28.33	71.67	0.00	100.00
9	12.57	87.43	100.00	28.04	71.62	0.34	100.00
AVE	12.45	87.55	100.00	28.35	71.58	0.08	100.00
STD	0.56	0.57		0.14	0.12	0.13	

E13C26							
	Galena			**Sphalerite**			
Analysis	**S wt%**	**Pb wt%**	**Total**	**S wt%**	**Zn wt%**	**Fe wt%**	**Total**
1	12.07	87.93	100.00	28.7	71.3	0.00	100.00
2	11.77	88.23	100.00	29.23	70.77	0.00	100.00
3	12.01	87.99	100.00	28.63	71.37	0.00	100.00
4	12.44	87.56	100.00	29.37	70.63	0.00	100.00
5	12.37	87.63	100.00	26.57	73.43	0.00	100.00
6	12.19	87.81	100.00	29.02	70.7	0.28	100.00
7	12.14	87.86	100.00	28.84	70.69	0.47	100.00
8	12.53	87.47	100.00	28.9	70.78	0.32	100.00
9	11.98	88.02	100.00	28.95	71.05	0.00	100.00
10	12.36	87.64	100.00	28.76	71.24	0.00	100.00
AVE	12.19	87.81	100.00	28.70	71.20	0.11	100.00
STD	0.23	0.23		0.74	0.79	0.17	

E14C27		
	Galena	**Sphalerite**

Analysis	S wt%	Pb wt%	Total	S wt%	Zn wt%	Fe wt%	Total
1	11.79	88.21	100.00	28.39	71.61	0.00	100.00
2	12.29	87.71	100.00	28.43	71.16	0.41	100.00
3	11.60	88.40	100.00	27.57	71.93	0.5	100.00
4	13.20	86.80	100.00	28.7	71.3	0.00	100.00
5	11.98	88.02	100.00	28.36	71.64	0.00	100.00
6	12.29	87.71	100.00	29.43	70.57	0.00	100.00
7	12.48	87.52	100.00	28.72	70.95	0.33	100.00
8	12.36	87.64	100.00	28.74	70.86	0.4	100.00
9	12.40	87.60	100.00	28.39	71.61	0.00	100.00
AVE	12.27	87.73	100.00	28.53	71.29	0.18	100.00
STD	0.43	0.43		0.46	0.42	0.21	

E14C28							
	Galena			**Sphalerite**			
Analysis	**S wt%**	**Pb wt%**	**Total**	**S wt%**	**Zn wt%**	**Fe wt%**	**Total**
1	11.21	88.79	100.00	27.79	72.21	0.00	100.00
2	11.85	88.15	100.00	27.97	72.03	0.00	100.00
3	11.55	88.45	100.00	28.21	71.79	0.00	100.00
4	12.14	87.86	100.00	28.04	71.96	0.00	100.00
5	11.53	88.47	100.00	28.77	71.23	0.00	100.00
6	12.97	87.03	100.00	27.71	72.29	0.00	100.00
7	12.09	87.91	100.00	28.38	71.34	0.28	100.00
8	11.78	88.22	100.00	28.44	71.14	0.42	100.00
9	12.86	87.14	100.00	28.04	71.96	0.00	100.00
AVE	12.00	88.00	100.00	28.15	71.77	0.08	100.00
STD	0.56	0.56		0.32	0.41	0.15	

E15C29							
	Galena			**Sphalerite**			
Analysis	**S wt%**	**Pb wt%**	**Total**	**S wt%**	**Zn wt%**	**Fe wt%**	**Total**
1	12.20	87.80	100.00	27.56	72.44	0.00	100.00
2	11.73	88.27	100.00	29.4	70.6	0.00	100.00
3	11.89	88.11	100.00	29.47	70.53	0.00	100.00
4	11.77	88.23	100.00	29.93	70.07	0.00	100.00
5	11.63	88.37	100.00	28.34	71.26	0.4	100.00
6	12.51	87.49	100.00	28.08	71.6	0.32	100.00
7	11.81	88.19	100.00	27.54	72.19	0.27	100.00
8	11.74	88.26	100.00	29.53	70.47	0.00	100.00
9	12.71	87.29	100.00	27.9	72.1	0.00	100.00
10	13.36	86.64	100.00	29.3	70.7	0.00	100.00

AVE	12.14	87.87	100.00	28.71	71.20	0.10	100.00
STD	0.53	0.53		0.86	0.80	0.15	